THE EFFECT OF LONG-TERM HIGH-FAT DIET FEEDING ON INTESTINAL HEALTH OF AGED VERVET MONKEYS

by

RONALDO MUKHARI

Dissertation

Submitted in fulfilment of the requirements of the degree of

MASTER OF SCIENCE

in

BIOCHEMISTRY

in the

FACULTY OF SCIENCE AND AGRICULTURE

(School of Molecular and Life Science)

at the

UNIVERSITY OF LIMPOPO

SUPERVISOR: Prof. V.G. Mbazima

CO-SUPERVISORS: Dr S. Riedel (SAMRC)

Prof. C.J.F. Muller (SAMRC)

2024

DEDICATION

This work is dedicated to myself, for the persistence, drive, discipline, lessons, skills and experience I have come to learn and acquire.

DECLARATION

I declare that the study entitled "THE EFFECT OF LONG-TERM HIGH-FAT DIET FEEDING ON INTESTINAL HEALTH OF AGED VERVET MONKEYS" is my own work and has not been submitted before for any other degree at any other institution of higher learning. I further declare that all the sources I have used or quoted have been indicated and acknowledged by complete references.

Ronaldo Mukhari   15 May 2023

Full names   **Date**

ACKNOWLEDGEMENTS

ABSTRACT

The consumption of Westernised high-fat diets (HFDs) dysregulates intestinal barrier components which may lead to subclinical systemic and tissue inflammation implicated in type 2 diabetes (T2D) development. It is essential to understand the intestinal barrier's role in developing T2D. This may aid in the identification of potential therapeutic and preventative targets for intestinal barrier defects and downstream metabolic impairments. This study investigated intestinal barrier function and inflammation in intestinal tissues of vervet monkeys (*Chlorocebus aethiops*) towards the development of T2D. The study made use of intestinal tissues (duodenum, jejunum, ileum and colon) and serum that was previously collected from nine vervet monkeys that were maintained on a maize-based control diet (MD) (n=3) and an HFD (n=6), respectively for 15 years. Serum was used to assess glycaemic and lipogram parameters. Haematoxylin and Eosin (H&E) staining was used for general morphological assessment and immunohistochemistry (IHC) was used to assess the expression of intestinal immunity marker, immunoglobulin-A-positive (IgA$^+$) cells of the duodenum, jejunum, ileum and colon. IHC was also used to assess the expression of intestinal barrier integrity marker, occludin in the ileum and colon. Western blot analysis was used to assess the expression levels of markers that are involved in the synthesis of pro-inflammatory mediators, extracellular signal-regulated kinase 1/2 (ERK1/2) and p38 in the ileum and colon. The expression levels of leaky gut biomarkers in serum: lipopolysaccharide-binding protein (LBP) and cluster of differentiation 14 (CD14) were assessed using respective enzyme-linked immunosorbent assay (ELISA) kits. The results revealed that the HFD did not induce significant changes in fasting blood glucose nor glycated haemoglobin levels of the vervet monkeys when compared to MD-fed vervet monkeys. There were no significant changes in triglyceride between HFD-fed and MD-fed vervet monkeys. Furthermore, total cholesterol levels were marginally increased (p=0.071), high-density lipoprotein cholesterol and low-density lipoprotein cholesterol levels were significantly increased (p=0.048 and p=0.017 respectively) in HFD-fed vervet monkeys as compared to MD-fed monkeys. H&E staining revealed that an HFD did not affect the morphology of the ileum and colon of vervet monkeys as evidenced by no significant changes in the villus length and crypt depth respectively when compared to MD-fed vervet monkeys. Immunohistochemical analysis revealed that an HFD significantly increased (p=0.046)

the population of IgA$^+$ cells in the duodenum of vervet monkeys when compared to MD-fed vervet monkeys. However, no significant changes in the population of IgA$^+$ cells were demonstrated in the jejunum, ileum and colon between HFD-fed and MD-fed vervet monkeys. HFD-fed vervet monkeys did not demonstrate significant changes in the expression of occludin in the ileum and colon when compared to MD-fed vervet monkeys. Western blot analysis revealed that there were no significant changes in the expression of ERK1/2 and p38 in the ileum and colon between HFD-fed and MD-fed vervet monkeys. There were no significant differences in serum levels of LBP and CD14 assessed by ELISA between HFD-fed and MD-fed vervet monkeys. In conclusion, this study demonstrated that an HFD dysregulated lipid metabolism in HFD-fed vervet monkeys, suggesting a probable predisposition to developing metabolic disease. In addition, the increased population of IgA$^+$ cells in the duodenum of HFD-fed vervet monkeys suggests dysregulated mucosal immunity. However, further research is warranted to elucidate underlying mechanisms.

TABLE OF CONTENTS

LIST OF FIGURES

LIST OF TABLES

LIST OF CONFERENCES AND PRESENTATIONS

Mukhari R., , Muller C.J.F., Mbazima V.G and Riedel S. The effect of long-term high-fat diet feeding on intestinal health of aged vervet monkeys. 55th Society for Endocrinology, Metabolism and Diabetes of South Africa Congress, Lagoon Beach Hotel, Cape Town, September 09-11, 2022 (poster presentation).

Mukhari R., , Muller C.J.F., Mbazima V.G. and Riedel S. The effect of long-term high-fat diet feeding on intestinal health of aged vervet monkeys. 12th Annual BRIP Research Symposium, SAMRC Conference Centre, Cape Town, October 18-19, 2022 (oral presentation).

LIST OF ABBREVIATIONS

µg – Microgram

µL – Microlitre

°C – Degree Celsius

AMP – Anti-microbial peptide

AREC – Animal Research Ethics Committee

APS – Ammonium persulfate

BRIP – Biomedical Research and Innovation Platform

BSA – Bovine serum albumin

CAF – Central Analytical Facility

CD14 – Cluster of differentiation 14

Cox – Cyclo-oxygenase

DC – Dendritic cell

dH_2O – Distilled water

ECRA – Ethics Committee for Research on Animals

ELISA – Enzyme-Linked Immunosorbent Assay

ERK – Extracellular signal-regulated kinase

FBG – Fasting blood glucose

FOXP3 – Forkhead box P3

GALT – Gut-associated lymphoid tissue

HbA1c – Glycated haemoglobin

H&E – Haematoxylin and Eosin

HDL-C – High-density lipoprotein cholesterol

HFD – High-fat diet

HFHSD – High-fat high-sugar diet

HRP – Horseradish peroxidase

Ig – Immunoglobulin

IgR – Immunoglobulin receptor

IL – Interleukin

IEC – Intestinal epithelial cell

IESC – Intestinal epithelial stem cell

JAM – Junctional adhesion molecule

kDa – Kilodalton

kg – Kilogram

L – Litre

LDL-C – Low-density lipoprotein cholesterol

LPS – Lipopolysaccharide

LBP – LPS-binding protein

mAb – Monoclonal antibody

MAPK – Mitogen activated protein kinase

MD – Maize-based diet

mg – Milligram

mL – Millilitre

MLN – Mesenteric lymph node

mm – Millimetre

mmol – Millimole

MUC2 – Mucin 2

MyD88 – Myeloid differentiation primary response protein 88

NBF – Neutral buffered formalin

ND – Normal diet

NHP – Nonhuman primate

NF-κB – Nuclear Factor kappa B

ng – Nanogram

NGS – Normal goat serum

PAMP – Pathogen associated molecular pattern

PBS – Phosphate buffered saline

pIgA – Polymeric IgA

pIgR – Polymeric immunoglobulin receptor

PRR – Pathogen recognition receptor

PUDAC – Primal Unit and Delft Animal Centre

PVDF – Polyvinylidene fluoride

px – pixel

RIP3 – Receptor-interacting protein kinase 3

ROI – Region of interest

rpm – Rotations per minute

SAMRC – South African Medical Research Council

SD – Standard deviation

SDS – Sodium dodecyl sulfate

SED – Subepithelial domain

sIgA – Secretory immunoglobulin A

T2D – Type two diabetes

TBS – Tris buffered saline

TC – Total cholesterol

TG – Triglyceride

TJ – Tight junction

TEMED – N, N, N', N' Tetramethylethylene-1,2-diamine

TIFF – Tagged Image File Format

TLR – Toll-like receptor

TNF-α – Tumour necrosis factor alpha

WD – Westernised diet

ZO – Zonula occludens

CHAPTER ONE

1. Introduction

The consumption of Westernised high-fat diets (HFD) has increased in middle and high-income countries. Indeed, an HFD evokes pathological changes in lipid and energy metabolism as well as an inflammatory state and potentiates the development of type 2 diabetes (T2D) (Christ *et al.*, 2019). Type 2 diabetes is a metabolic disease characterised by chronic high glucose blood levels as a result of impaired insulin sensitivity and insulin production (Roden and Shulman, 2019). The prevalence and incidence of T2D are rising due to obesity, ageing (Chatterjee *et al.*, 2017; Zhou *et al.*, 2016) and an unhealthy diet (Malesza *et al.*, 2021). Seemingly, disruption of intestinal barrier components of the mucosa by an HFD leads to inflammation that may contribute to the development of T2D and its complications (Khoshbin and Camilleri, 2020; Mohammad and Thiemermann, 2021; Winer *et al.*, 2017).

While the precise mechanisms of HFD-associated inflammation are complex and need further elucidation (Malesza *et al.*, 2021), Luck *et al.* (2019) reported that an HFD led to a decrease in the amount of immunoglobulin-A-positive (IgA$^+$) cells in the colon of mice. The reduction of IgA$^+$ cells was associated with impaired glucose metabolism. Winer *et al.* (2017) compressively described the alterations in immune cell populations as a result of HFDs and development of a predisposition to metabolic disease. Lipopolysaccharide (LPS), an endotoxin that is found in the intestinal lumen (Rhee, 2014), was reported to have accumulated in the systemic circulation of mice fed an HFD as a result of increased intestinal permeability (Cani *et al.*, 2008). Consequently, the accumulation of LPS in systemic circulation (metabolic endotoxemia) influenced a chronic pro-inflammatory state triggered by pro-inflammatory cytokines (Cani *et al.*, 2007). Cani *et al.* (2012) reported that the expression of intestinal barrier integrity markers, tight junction (TJ) proteins, were deregulated in HFD-fed mice, leading to increased intestinal permeability. Therefore, it is evident that an HFD can exert local and systemic inflammation associated with T2D as a result of impaired intestinal barrier function. This may lead to the identification of diagnostic and therapeutic targets to prevent and/or ameliorate the development of T2D and its associated complications.

Non-human primates (NHPs), such as vervet monkeys, have a close association with humans with regard to clinical and pathological features of T2D (Pound *et al.*, 2014), making them a suitable animal model for investigating the long-term effects of an HFD on intestinal tissues of an aged population of vervet monkeys.

1.1. Purpose of the study

1.1.1. Aim

To investigate the role of long-term feeding of a Westernised high-fat diet on the intestinal barrier function and inflammation in intestinal tissues of vervet monkeys towards the development of type 2 diabetes (T2D).

1.1.2. Objectives

To achieve this aim, the effect of a Westernised high-fat diet in the tissues of vervet monkeys was assessed with a specific focus on:

I. morphology of intestinal tissues using Haematoxylin and Eosin (H&E) staining.
II. intestinal barrier function, intestinal immune cell population and inflammation in intestinal tissues using Immunohistochemistry and western blot.
III. serum markers of intestinal barrier dysfunction in vervet monkeys using Enzyme-Linked Immunosorbent Assay (ELISA).

1.1.3. Hypotheses

I. Long-term feeding of a Westernised high-fat diet leads to intestinal barrier dysfunction due to the deregulation of the expression of tight junction proteins in intestinal tissues of aged vervet monkeys.
II. Long-term feeding of a Westernised high-fat diet increases the levels of markers of intestinal barrier dysfunction in the serum of aged vervet monkeys.

CHAPTER TWO

2. Literature review

2.1. Intestinal barrier composition and function

The intestine is one of the largest regions of the human body that is in contact with the external environment (Artis, 2008). The mucosa of the small intestine has finger-like projections known as villi which are covered by a monolayer of intestinal epithelial cells (IECs). Villi form shallow invaginations known as crypts of Lieberkühn. The mucosa of the large intestine is devoid of villi and made up of crypts. Altogether, these structures provide the intestine with digestive and absorptive (mainly in the small intestine) capabilities and form a defensive barrier. The intestinal barrier protects the human body from luminal contents such as toxins and dietary antigens (König *et al.*, 2016; Salvo Romero *et al.*, 2015; Sherwood, 2010). The mucosa of the intestine is lined with intestinal epithelial cells (IECs) that produce enzymes, peptides and proteins, and provides the mucus that protects the epithelium (Eri and Chieppa, 2013). Components of the intestinal barrier can be categorised into the physical barrier, chemical barrier and immunological barrier based on their anatomical location and function. Intestinal epithelial cells are held together by protein complexes known as tight junctions (TJs) that prevent paracellular permeability of pathogens, toxins and dietary antigens forming a physical barrier (Balda and Matter, 2008). The chemical barrier removes or neutralises antigens and microorganisms found in the lumen (Okumura and Takeda, 2017). The constant exposure of the intestines to pathogens, toxins and dietary antigens warrants immunological protection. Intestinal epithelial cells along with immune cells of the gut-associated lymphoid tissue (GALT) work together to form an immunological barrier. All these components are crucial to prevent ailments and diseases, including T2D and its co-morbidities (Maldonado-Contreras and McCormick, 2011; Mowat and Agace, 2014).

2.1.1. Physical barrier

The physical barrier, also referred to as the mechanical barrier, acts as a physical barrier against luminal content (Qin *et al.*, 2008). It is made up of various components such as the outer and inner mucus layers, IECs, and protein complexes between IECs known as tight TJ proteins (Balda and Matter, 2008; Ermund *et al.*, 2013). The outer mucus layer is loose, rich in antibacterial peptides and prevents invasion by microorganisms into the epithelial layer (Antoni *et al.*, 2013). The inner mucus layer is

firmly attached to the epithelial layer and it also prevents permeation by microorganisms (Ghosh, 2020).

There are various types of IECs, these include enterocytes, Paneth cells, goblet cells, and enteroendocrine cells **(Figure 2.1)**. All IECs arise from intestinal epithelial stem cells found within the crypts of Lieberkühn. Under normal physiological conditions, IECs become senescent and are shredded from the epithelium into the lumen, and therefore must be renewed by intestinal epithelial stem cells found at the base of invaginations or crypts (Booth and Potten, 2000; Marshman *et al.*, 2002). Enterocytes are the most abundant IECs, and they are not only involved in the absorptive functions of the intestine but also the release of antimicrobial proteins. Enterocytes also play a role in inducing immune tolerance to antigens in the lumen (Miron and Cristea, 2012), including the release of cytokines and chemokines (Zeuthen *et al.*, 2008). Above the microvillar surface of enterocytes lies a layer made up of carbohydrate moieties of glycoproteins or glycolipids including transmembrane proteins, termed the glycocalyx layer. The glycocalyx layer resides between the intestinal epithelium and mucus layer, and it covers and protects epithelial cells from pathogenic microorganisms. Both the glycocalyx layer and mucus layer are made up of oligosaccharides that cannot be cleaved by host glycosidases, thus they protect the intestinal environment from auto-digestion (Pelaseyed *et al.*, 2014; Sun *et al.*, 2020). The glycocalyx layer may serve as an attachment site for microorganisms that reside in the lumen due to its composition of glycoproteins such as mucins which may serve as receptors for bacterial attachment (Hansson, 2020). Goblet cells release mucus, glycoproteins and cytokines for maintaining intestinal epithelium homeostasis (Kim and Ho, 2010; Birchenough *et al.*, 2015). Paneth cells which are found in the small intestine are responsible for the production of antimicrobial peptides (AMPs) as well as inflammatory mediators and signalling molecules (Keshav, 2006). Enteroendocrine cells exude peptide hormones required for digestion (Worthington, 2015). These IECs are held together by a polarised layer of TJs, adhesion junctions and desmosomes which are connected to an actin skeleton to form an efficient physical barrier (Balda and Matter, 2008; Hao *et al.*, 2022).

TJ proteins are complex, multiprotein structures located between plasma membranes of epithelial cells that are responsible for permitting the transport of water-soluble molecules across the epithelium by creating a physical barrier that holds the epithelial

cells together (Balda and Matter, 2008). The protein complexes include junctional adhesion molecules (JAMs), scaffolding proteins such as zonula occludens (ZO)-1, -2, and -3, and transmembrane proteins such as occludin and claudins (Garcia *et al.*, 2018; Hao *et al.*, 2022). The family of transmembrane proteins, claudins, are involved in preventing the unregulated paracellular permeability of water and solutes including luminal toxins and antigens across the epithelium (Rosenthal *et al.*, 2010). Claudins colocalise with ZO proteins (Holmes *et al.*, 2006), and the interaction of ZO proteins with other transmembrane proteins is crucial for the proper functioning of the intestinal barrier. Zonula occludens proteins are also involved in regulating cell proliferation (Garcia *et al.*, 2018). Occludin also colocalises with ZO-1, -2, and -3, and has been reported to be involved in regulating paracellular permeability, tight junction assembly, and cell-cell adhesion (Balda *et al.*, 1996; Chen *et al.*, 1997; Van Itallie and Anderson, 1997).

Within the intestinal lumen, secretory Immunoglobulin A (sIgA) is involved in directly immobilising luminal contents by a process known as immune exclusion. Although sIgA is an immunological component of the barrier, it achieves its defence functionality through "physical means". Immune exclusion of antigens and pathogens can be characterised by agglutination, entrapment in mucus and clearance through peristalsis (Deplancke and Gaskins, 2001; Liévin-Le Moal and Servin, 2006; Mantis and Forbes, 2010).

2.1.2. Chemical barrier

Based on its composition and contents, the intestinal lumen, forms the chemical barrier, and it is the site where antigens and microorganisms are inactivated by pH, gastric, pancreatic, and biliary secretions (Sarker and Gyr, 1992). The intestinal lumen consists of mucus containing intestinal alkaline phosphatase and antimicrobial peptides (AMPs) (Keshav, 2006; Pietrzak *et al.*, 2020).

The mucus layer is rich in mucins, specifically mucin 2 (MUC2), which is involved in regulating the propensity of invasion and localisation of pathogens onto the intestinal mucosa of murines (Bergstrom *et al.*, 2010; Hasnain *et al.*, 2010). Intestinal alkaline phosphatase is an important enzyme that hydrolyses several substates within the intestinal lumen (Engle *et al.*, 1995). Intestinal alkaline phosphatase executes its defensive role by attenuating the activity of luminal endotoxins such as LPS (Poelstra

and Bakker, 1997). Other components of the chemical barrier include AMPs, which are small proteins released by Paneth cells to detect and protect against bacteria and bacterial products. Examples of AMPs include defensins, cathelicidins and lysozyme (Ehmann *et al.*, 2019; Gieryńska *et al.*, 2022). AMPs have been reported to exhibit immunomodulatory activity *in vivo* and *in vitro* as well as antibacterial activity. For instance, the human AMP, LL-37, prevented LPS activity by inhibiting the expression of the pro-inflammatory cytokine, tumour necrosis factor α (TNF-α) in monocytic cells (Niyonsaba *et al.*, 2002; Mookherjee *et al.*, 2006) while lysozyme is known for inducing bacterial lysis (Ragland and Criss, 2017). All these chemical components are essential for the maintenance and protection of the health of the host from pathogens.

2.1.3. Immunological barrier

The intestinal epithelium with associated lymphocytes, the lamina propria and GALTs are the major regions of the intestine that form the immunological barrier. The GALT consists of specialised tissues or organs such as organised lymphoid tissues (Peyer's patches), isolated lymphoid follicles and mesenteric lymph nodes (MLNs) found in different regions along the intestines (Hamada *et al.*, 2002; Mowat and Agace, 2014).

Below the basolateral membrane of IECs is a lymphoid area known as Peyer's patches (PPs). Peyer's patches reside in the subepithelial domain, a dome-like structure found beneath the epithelium characterised by a large population of lymphocytes, macrophages and dendritic cells **(Figure 2.1)** (Mowat and Agace, 2014). They are also a site of plasma B cell maturation and are regarded to greatly contribute to the induction of IgA response (Williams, 2006; Velaga *et al.*, 2009). Isolated lymphoid follicles occur throughout the length of the intestine even though there are differences in their density, cellular composition, and location along intestinal segments. They are much smaller than PPs and are reported to be capable of inducing adaptive immune responses of the gut. The lymph coming from the intestine is filtered by MLNs of the GALT which may initiate immune responses against antigens. Mesenteric lymph nodes also work with DCs that migrate from the lamina propria in initiating immune responses against antigens (Ahluwalia *et al.*, 2017; Fenton *et al.*, 2020; Mörbe *et al.*, 2021).

Gut-associated lymphoid tissue immune cells such as macrophages and DCs including IECs are equipped with pattern-recognition receptors (PRRs), which enable

binding with pathogen-associated molecular patterns (PAMPs). Pathogen-associated molecular patterns are ligands found in both pathogenic and commensal microbiota and they associate with PRRs when microorganisms invade the intestinal epithelium. Stimulation of PRRs such as Toll-like receptor-2 (TLR2), TLR3 and TLR4 expressed in the small and large intestine under normal physiological conditions by luminal content elicit host defence mechanisms (Bogunovic *et al.*, 2007; Cario and Podolsky, 2000; Otte *et al.*, 2004). Toll-like receptor-4 stimulation by the bacterial endotoxin, LPS, is initiated firstly by recognition of LPS-binding protein (LBP) which binds with the lipid A tail of LPS to facilitate the interaction of LPS with a receptor in myeloid cells, cluster of differentiation 14 (CD14) (Pugin *et al.*, 1993). Myeloid differentiation protein-2 (MD-2) then allows the detection of LPS by TLR4 (Shimazu *et al.*, 1999; Viriyakosol *et al.*, 2001). Activation of this complex triggers the innate immune response against potentially invasive microbiota and serves as a host defence mechanism. For instance, upon TLRs stimulation, adaptor molecules such as MyD88 and TIR-domain-containing adapter-inducing interferon-β are recruited to initiate signal transduction pathways that lead to the activation of nuclear factor-κB (NF-κB), interferon regulatory factors or mitogen-activated protein kinases (MAPKs). These molecules regulate the expression of cytokines, chemokines and type I interferons (Choi *et al.*, 2010).

Another immunological component of the barrier is a population of lymphocytes known as intraepithelial lymphocytes (IELs) that form part of IECs. These are in direct contact with luminal antigens and elicit defensive immune responses such as protective immunity against pathogens including prevention of intestinal damage by pathogens (Cheroutre *et al.*, 2011; Roberts and Hayday, 1996). Microfold cells arising from GALTs form part of IECs. They are distinct from other IECs in that they have a microfold instead of microvilli on their apical surface (Miller, 2007). Furthermore, they have an invaginated basolateral membrane which harbours a population of lymphocytes (Regoli *et al.*, 1995). They are mainly involved in the transportation of luminal substances to the underlying tissues of the mucosal immune system for sampling by antigen-presenting cells (Mowat, 2003). Beneath the single layer of IECs lies a region of connective tissue known as the lamina propria **(Figure 2.1)**. The lamina propria is a site that contains a large population of immune cells such as CD4$^+$ T-cells, CD8$^+$ T-cells, and IgA-producing plasma B-cells (Fagarasan and Honjo, 2003; Wershil and Furuta, 2008). The CD4$^+$ T cells found within this region express several cytokines

such as interleukin (IL)-2, IL-10 and IL-17. CD4^{+} T regulatory cells express IL-10 and the transcription factor forkhead box P3 (FOXP3). FOXP3 is an important transcription factor that plays a role in T regulatory cell differentiation. Seemingly, T regulatory cells suppress unwanted immune responses triggered by antigens thereby preventing autoimmunity and pathology which may arise if not regulated (Sathaliyawala *et al.*, 2013; Veenbergen and Samsom, 2012; Zheng and Rudensky, 2007). The lamina propria is also home to several DCs, eosinophils, macrophages and mast cells (Acheson and Luccioli, 2004). These cells have essential roles in eliciting immuno-protective responses within the intestinal barrier.

Plasma B cells within the mucosa of the intestine release IgA both in the small and large intestines (Brandtzaeg and Johansen, 2005). The IgA found in the intestinal lumen is the most abundant immunoglobulin whereas serum IgA is the second most predominant type of immunoglobulin in blood circulation (Conley, 1987; Mestecky *et al.*, 1986). Mucosal plasma B cells produce a polymeric IgA (pIgA), which is basically an aggregate of monomeric IgA antibodies linked together at the Fc portion of antibodies by a J chain (Leong and Ding, 2014). Along the basolateral membrane of IECs, pIgA binds with a polymeric immunoglobulin receptor (pIgR), which facilitates pIgA's transportation across the epithelium to mucosal surfaces. Upon reaching mucosal surfaces, the bound pIgA is released from pIgR into the intestinal lumen as a dimeric form of IgA known as sIgA that is bound to a glycoprotein, secretory component, derived from the pIgR (Pabst, 2012). Immunoglobulin A produced in the gut has key functions such as regulation of antigen transport and uptake, immunomodulatory properties through binding IgA-receptors, and the aforementioned function, "immune exclusion" of pathogens and antigens. Additionally, sIgA is one of the first lines of defence in the lumen and prevents intestinal antigens (e.g. food, pathogens, self-antigens) from reaching the submucosa and systemic circulation **(Figure 2.1)** (Gommerman *et al.*, 2014).

Within the intestinal barrier, IgA can regulate innate and adaptive immunity functions by interacting with host receptors of myeloid, lymphoid and non-haemopoietic cells (Woof and Russell, 2011). Additionally, sIgA has been reported to directly interact with, and neutralise microorganisms to prevent entry across the epithelium (de Sousa-Pereira and Woof, 2019). During transcytosis of IgA across the epithelium, IgA was shown to attenuate the pro-inflammatory activity of LPS (Fernandez *et al.*, 2003),

suggesting its role in inducing anti-inflammatory activity. Moreover, multiple attachment sites on sIgA permit it to form crosslinks with antigens entrapping them in the mucus, thus preventing entry across the epithelium (Mantis *et al.*, 2011; de Sousa-Pereira and Woof, 2019), further avowing its importance in the regulation of the intestinal barrier. Components of the GALT including those of the physical and chemical barrier work together to form an efficient intestinal barrier. However, this barrier can be compromised by dietary antigens from the consumption of an unhealthy diet such as an HFD.
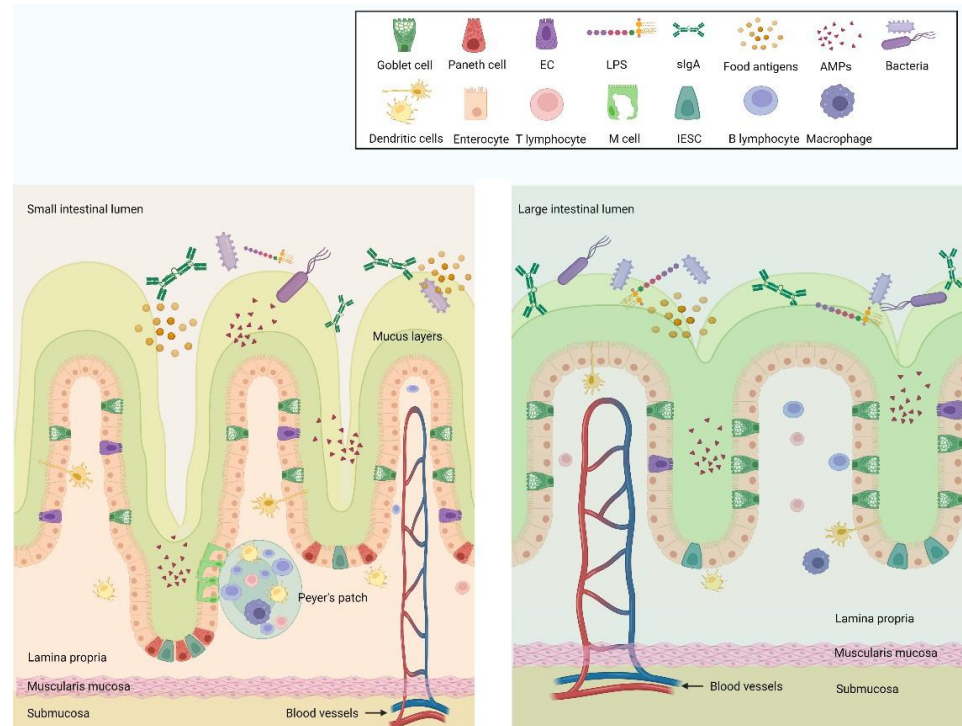
Figure 2.1: : Intestinal barrier components in the small and large intestines. The intestinal lumen is a site of endogenous and exogenous material such as food antigens, bacteria and bacterial products such as lipopolysaccharide (LPS). An epithelial layer lines the intestinal wall with enterocytes, enteroendocrine cells (ECs), M cells, intestinal epithelial stem cells (IESCs) including goblet cells which maintain mucus layers. The mucus layer immobilises unwanted foreign material, antimicrobial products (AMPs) released by Paneth cells and secretory IgA (sIgA) released by B cells to remove or prevent the unwanted foreign material from passing the epithelium and ultimately into systemic circulation. Peyer's patches contain immune cells such as lymphocytes, macrophages and dendritic cells. The image was adapted from Mohammad and Thiemermann (2021) and created in Biorender

2.2. Effects of a high-fat diet on intestinal barrier components

Westernised diets (WDs) are unhealthy calorie-dense foods enriched in simple carbohydrates and saturated fats such as processed foods, convenience products and snacks, but lacking fibre vitamins and minerals (Christ *et al.*, 2019; Mozaffarian, 2016). In addition, the total calories from Westernised HFDs range from 37-72% (Malesza *et al.*, 2021). Over the last decades, there has been an increase in the consumption of WDs, particularly HFDs in high-income countries, as well as middle-income countries. This trend has been correlated to the increase in the incidence and prevalence of T2D as well as inflammation (Christ *et al.*, 2019; Imamura *et al.*, 2015). The metabolic complications associated with this are subclinical systemic and tissue inflammation (Genser *et al.*, 2018). As such an HFD can impair or dysregulate intestinal barrier components such as the gut microbiota, IECs, TJ protein functions, and cells of GALTs. These alterations may lead to changes in whole-body metabolism, increased intestinal permeability, and inflammation, and are associated with an increased predisposition to T2D (Cani *et al.*, 2007; Kim *et al.*, 2012).

2.2.1. Effects of a high-fat diet on intestinal tight junction protein complex and plasma cell populations

Deregulation of TJ protein complex activity has been implicated in increased intestinal permeability, for instance, mice fed an HFD had low ZO-1 and occludin expression levels when compared to mice fed a normal diet (ND). The decrease in the TJ proteins was associated with increased circulating levels of intestinal permeability biomarkers (Cani *et al.*, 2008). Germ-free mice fed an HFD were reported to have decreased expression of occludin when compared to ND-fed mice (Nakanishi *et al.*, 2021). The study also reported increased intestinal permeability as assessed by fluorescein isothiocyanate dextran assay in the HFD-fed mice. Another study found that an HFD in Otsuka Long Evans Tokushima Fatty obese rats and Long Evans Tokushima Otsuka lean counter rats, led to increased intestinal permeability evaluated by increased urinary excretion of chromium ethylenediaminetetraacetic acid and phenolsulfonphthalein levels. The authors further reported low expression of TJ proteins such as JAM-1, occludin, claudin-1 and claudin-3 in the small intestine. They further reported that the severity of these findings increased with age (Suzuki and Hara, 2010). A study by Okyere *et al.* (2022) demonstrated that mice fed an HFD had decreased expression and localisation of occludin in the small intestine when

compared to mice fed an ND. Shen *et al.* (2014) reported low expression levels of claudin-1 and occludin including decreased localisation of ZO-1 in the ileum of mice fed an HFD. These findings were associated with increased markers of ileal inflammation and systemic inflammation in the HFD group to suggest intestinal barrier dysfunction.

A study revealed decreased expression of IgA^{+} cells in the lamina propria of mice fed with an HFD in contrast to standard-diet-exposed mice (Sakamoto *et al.*, 2021). The authors also did morphometric and metabolic assessments to validate the pathophysiologies linked to T2D. They further suggested that more understanding of the mechanism(s) leading to decreased immune function in the context of T2D and its conditions is needed. Another study which also looked at the effects of an HFD on intestinal barrier function reported that an HFD decreased the level of sIgA activity on gut microbiota (Muhomah *et al.*, 2019). Hence, suggesting a decreased expression of IgA by plasma cells (IgA^{+} cells).

2.2.2. Effects of a high-fat diet on toll-like receptor 4 signalling pathway and inflammation

TLR4 is a single-domain transmembrane plasma-bound receptor that recognises the endotoxin, LPS, causing the release of pro-inflammatory cytokines. A marked increase in gut-derived LPS following HFD consumption is characteristic of metabolic endotoxemia (Cani *et al.*, 2007). Stimulation of TLR4 receptors by LPS leads to the downstream activation of MAPKs (Mohammad and Thiemermann, 2021). This eventually leads to activation of NF-κB which influences the expression of pro-inflammatory genes (Kawasaki and Kawai, 2014).

Consumption of an HFD in rats caused an increase in plasma LPS which was correlated with increased colonic TNF-α, Cyclooxygenase (COX-2) and NF-κB expression levels when compared with ND-fed rats (Kim *et al.*, 2012). The authors further reported that occludin and claudin-1 expression levels were decreased in the colon of HFD-fed mice when compared with ND-fed mice. This may have exacerbated the accumulation of gut-derived LPS into systemic circulation since TJ proteins regulate intestinal permeability. Similarly, Yu *et al.* (2020) reported that rats fed an HFD had increased serum LPS including increased expression levels of TNF-α and IL-1β in the colon when compared to rats fed an ND. They also reported decreased

expression levels of TJ proteins (ZO-1 and occludin) in the HFD-fed rats when compared with ND-fed mice. The TLR4 signalling pathway was more stimulated in rats fed an HFD than those fed an ND. This was due to increased ileal expression levels of TNF-α, TLR4 as well as the cell death regulator, receptor-interacting protein kinase 3 (RIP3), in HFD-fed rats as compared to the ND-fed rats. Immunohistochemical analysis revealed decreased expression of ileal ZO-1 and occludin in the HFD-fed group when compared to the ND diet group (Su *et al.*, 2019). Fang *et al.* (2017) demonstrated that an HFD in rats induced high expression levels of TLR4 and MyD88 in both the ileum and colon in contrast to the control group fed an ND.

There is a consensus in the literature that changes in intestinal morphology may serve as markers of intestinal inflammation (Peuhkuri *et al.*, 2010). Rats fed a high-fat high-sugar diet (HFHSD) had increased duodenal and jejunal villus height when compared to those fed an ND (Natali Almeida *et al.*, 2014). The HFHSD rats also had increased body weight and adiposity when compared with ND-fed rats. Numerous studies also reported that HFD-induced obesity in mice was associated with increases in duodenal and jejunal villus height when compared to mice fed an ND (Baldassano *et al.*, 2013; Mao *et al.*, 2013; Mah *et al.*, 2014). Mah *et al.* (2014) further reported that HFD-induced obesity in mice was correlated with hyperinsulinaemia, thus avowing the link between HFD and metabolic conditions including intestinal health.

Altogether, these studies support the possibility of an HFD impairing intestinal barrier function. This may lead to both systemic and intestinal inflammation which could give rise to obesity and T2D as a result of intestinal barrier dysfunction. However, more research on the effect of an HFD on different regions of the intestine (duodenum, jejunum, ileum and colon) needs to be conducted to elucidate the mechanistic effects diet may play on intestinal barrier components of these regions. Riedel *et al.* (2022) posited that there is a paucity of research on the involvement of intestinal barrier function and the immune function of GALT in the development of metabolic disorders.

2.3. Metabolic disorders and intestinal barrier dysfunction in non-human primates

Non-human primates have been used in research studies for over 50 years to elucidate the pathophysiology of metabolic diseases such as diabetes. The most used NHPs in research are from eight genera and are categorised into either Old-World

primates or New-World Primates. The Old-World primates include rhesus monkeys (*Macaca mulatta*), baboons (*Papio* spp.), African green monkeys (*Chlorocebus* spp.) and cynomolgus monkeys (*Macaca fascicularis*). Whereas, the New-World primates include owl monkeys (*Aotus* spp.), squirrel monkeys (*Saimiri* spp.), marmosets (*Callithrix* spp.) and tamarins (*Saguinus* spp.) (Havel *et al.*, 2017).

Non-human primates are an invaluable model in biomedical research. They offer an efficacious approach to understanding metabolic disorders. Also, they develop similar metabolic features such as obesity, insulin resistance, adiposity and hypertension present in humans (Pound *et al.*, 2014). They also have more similar characteristics to humans such as similar glucose and lipid metabolism activity including similar major classes of plasma lipoproteins (Havel *et al.*, 2017). Studies have also aimed to show that NHPs can also develop metabolic disease because of physical inactivity and an unhealthy diet. For instance, Higgins *et al.* (2010) reported that baboons fed an HFHSD had elevated levels of fat mass, triglyceride (TG) and glycated haemoglobin (HbA1c), indicative of metabolic syndrome. A group of rhesus monkeys fed an HFD developed impaired glucose tolerance, impaired fasting glucose over time, and eventually became obese (Gong *et al.*, 2013). Another group of rhesus monkeys fed a high-fructose diet developed metabolic syndrome features such as insulin resistance, adiposity and dyslipidaemia. This was characterised by increased plasma insulin levels, body weight and fat mass, and, increased fasting TG levels and decreased fasting high-density lipoprotein cholesterol (HDL-C) levels, respectively. Moreover, the high-fructose-fed monkeys depicted increased plasma levels of a pro-inflammatory marker, C-reactive protein (Bremer *et al.*, 2011), known to play a role in the pathophysiology of T2D. In another study, a group of cynomolgus monkeys fed an HFHSD demonstrated significant increases in TC and TG levels when compared to monkeys fed a normal (control) diet. Gene expression analysis further revealed that the high fat and sugar group had deregulated glucose and lipid metabolism (Jin *et al.*, 2019), which could have influenced increases in TC and TG levels. Another group of cynomolgus monkeys exposed to a WD developed adiposity and increased plasma insulin levels over time (Shively *et al.*, 2019). Common marmoset monkeys demonstrated that exposure to an HFHSD leads to adiposity, with increased plasma glucose and TG levels over time (Wachtman *et al.*, 2011).

Newman *et al.* (2021) reported that a WD in cynomolgus monkeys influenced a gut microbial profile that may be associated with sub-clinical inflammation when compared to Mediterranean-diet-fed cynomolgus monkeys. Another study reported that cynomolgus monkeys fed a WD had different lipid profiles associated with differences in their gut microbiota profiles (Gao *et al.*, 2022). Cynomolgus monkeys fed an HFD for 2.5 years had a high Firmicutes-Bacteroides ratio in their gut when compared to monkeys fed a Mediterranean diet. The HFD-fed group also had a higher abundance of *Clostridiacea* and *Lactobacillaceae* families (Nagpal *et al.*, 2018). Unfortunately, the authors did not investigate other intestinal barrier components such as TJ proteins and immune cell populations aside from the gut microbiota nor did they investigate the role of the gut microbiota composition on T2D risk factors such as inflammation. This indicates the elusive mechanistic impact of WDs on metabolic health including intestinal barrier function in the context of NHPs, accordingly, there is a paucity of research.

Indeed, disturbances in intestinal barrier function as a result of HFDs can lead translocation of harmful substances, contributing to chronic inflammation and metabolic disturbances. Hence, it is paramount to investigate the role of WDs on the intestinal health of NHPs to understand their role in the pathophysiology of T2D and its complications with the purpose to find diagnostic and therapeutic targets in humans.

CHAPTER THREE

3. Methodology and analytical procedures

3.1. Animal housing, husbandry, diet and sample collection

A population of vervet monkeys (*Chlorocebus aethiops*), housed at the Primate Unit and Delft Animal Centre (PUDAC), SAMRC, is routinely used for biomedical research. The vervet monkeys were housed in adherence to the South African National Standard for the Care and Use of Animals for Scientific Purposes (South African Bureau of Standards, SANS 10386, 2008). Subgroups of the monkey colony were maintained on a normal maize-based diet (MD) and a high-fat diet (HFD) (Fincham *et al.*, 1987) for over 15 years. The MD consisted of 14% of the energy derived from protein, 10% from fat, and 76% from carbohydrates and the HFD consisted of 14% of the energy derived from protein, 40% from fat and 46% from carbohydrates (Fincham *et al.*, 1987).

Once the animals reached 20 years of age and developed chronic diseases (Kavanagh *et al.*, 2007), they were no longer suited for biomedical research studies and were euthanised. This study utilised samples collected between 2017 and 2018, 3 monkeys on an MD and 6 on an HFD, aged (22.7 ± 2.3 years) (see **Table 6.4**), were euthanised and tissues collected. Monkeys were fasted overnight (16 hours), weighed and then anaesthetised with Ketamine (10 mg/kg body weight) for blood sample collection. Thereafter, sodium pentobarbital (400 mg/mL) was administered intravenously (2 mL/kg bodyweight) by registered and qualified staff at PUDAC to euthanise the monkeys. Tissues (duodenum, jejunum, ileum and colon) and blood were collected (6 mL in serum-separating tubes and 2 mL in sodium fluoride/ potassium oxalate tubes) by Drs Riedel and Chellan. The intestines were washed with phosphate-buffered saline (PBS) **(Table 6.2)** to remove faecal matter, snap-frozen in liquid nitrogen and stored at -80°C. For histological and immunohistochemical analysis **(Figure 3.1)**, tissues were fixed in 10% neutral buffered formalin (NBF) **(Table 6.2)**.

Ethical approval for the collection of tissues and blood of these animals was acquired from the SAMRC's Ethics Committee for Research on Animals (ECRA No 01/16) by Prof CJF Muller (BRIP, SAMRC). Ethical approval for the use of samples collected in this study was granted by the Animal Research Ethics Committee (AREC) from the

University of Limpopo, registered with the National Health Research Ethics Council (AREC-290914-017).
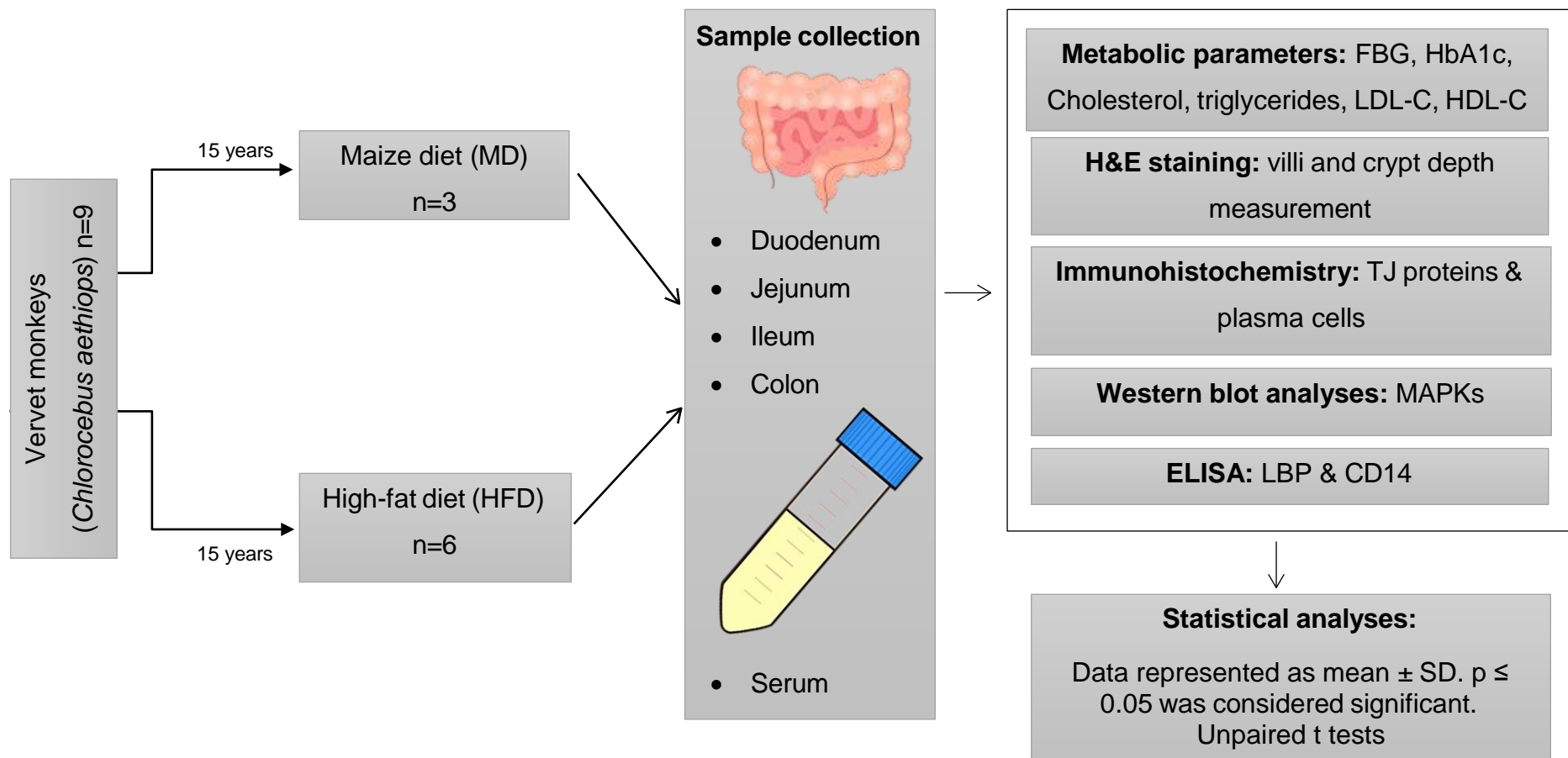
Figure 3.1: Study design— animal husbandry, diet and sample collection. Vervet monkeys (*Chlorocebus aethiops*) were maintained on either an MD (n=3) or an HFD (n=6) for more than 15 years. After reaching old age (>20 years), they were euthanised, tissues and blood samples were collected and stored for later use. Abbreviations: Haematoxylin and eosin (H&E), enzyme-linked immunosorbent assay (ELISA), fasting blood glucose (FBG), glycated haemoglobin (HbA1c), low-density lipoprotein cholesterol (LDL-C), high-density lipoprotein cholesterol (HDL-C), tight junction (TJ), mitogen-activated protein kinases (MAPKs), lipopolysaccharide (LPS), LPS-binding protein (LBP) and cluster of differentiation 14 (CD14).

3.2. Assessment of metabolic parameters (glycaemia and lipogram)

Collected blood samples from vervet monkeys **(described in section 3.1)** were centrifuged at 3300 x g at 4°C for 15 minutes and serum was collected and stored at -80°C by Mrs Charna Chapman at BRIP, SAMRC for later use. Analysis of glycaemic and lipogram parameters was conducted by PathCare laboratories (Cape Town, South Africa) before this study. Tests for glycaemic parameters included fasting blood glucose (FBG) and glycated haemoglobin (HbA1c) levels, and lipogram tests included total cholesterol (TC), triglyceride (TG), low-density lipoprotein cholesterol (LDL-C), and high-density lipoprotein cholesterol (HDL-C) levels. The data were represented as mean ± standard deviation (SD).

3.3. Preparation of tissue for histology

3.3.1. Tissue processing

The 10% NBF-fixed intestinal tissues were processed with the Leica TP1020 Automatic Tissue Processor **(Table 6.1)** by dehydrating in ascending concentrations of ethanol (70%, 96% and 100%), clearing in xylene **(Table 6.2)** and embedding with paraffin wax. Mrs C Chapman kindly completed the tissue processing between 2017 and 2018 prior to this study.

3.3.2. Tissue sectioning

Mr D Linden kindly sectioned the required tissues for this study. Briefly, the paraffin wax-embedded tissues (wax blocks) were cut into 5 µm sections using a Leica RM2125 RT Rotary Microtome **(Table 6.1)**. The sections were floated onto a water bath (25-30°C) and then placed onto microscopy slides **(Table 6.2)**.

3.4. Histological assessment of intestinal tissues using Haematoxylin and Eosin staining

Haematoxylin and Eosin (H&E) staining was used for general morphological assessment of intestinal tissues. Haematoxylin is a basic blue-purple dye that stains acidic components of the cell such as nucleic acids found in the nucleus. Eosin on the other hand is an acidic pink dye that stains basic components of the cell such as the cytoplasm or proteins non-specifically (Eroschenko and Fiore, 2013). Briefly, slides were placed in an incubator at 60ºC for 30 minutes to melt the wax. Thereafter, the wax on the slides was removed by placing them in xylene twice for 10 minutes. The xylene was removed with 100% ethanol and the sections hydrated in 95% ethanol (two

times) for two minutes. The slides were dipped 20 times in distilled water followed by staining with haematoxylin **(Table 6.2)** for 12 minutes. Thereafter, the sections were rinsed by dipping them in distilled water 10 times. Then, washed with tap water for 10 minutes and stained in 1% aqueous eosin **(Table 6.2)** acidified with acetic acid (**Table 6.2**) for two minutes. The slides were then rinsed by dipping them 20 times in distilled water and dehydrating them by dipping them in 95% ethanol (20 times) and placing them in two changes of 100% ethanol. Lastly, they were placed in xylene and then kept in xylene before mounting on coverslips with Entellan rapid mounting medium **(Table 6.2)** for imaging.

3.4.1. Imaging

The slides were imaged using a Nikon Eclipse Ti-S inverted microscope equipped with a Nikon Digital Sight DS-U3 camera and a Nikon Objective Plan Fluor 10x/0.30 objective **(Table 6.1)**. NIS-Elements software version 4.51.00 Build 1143 **(Table 6.1)** was used to acquire images. The camera was set to a high resolution of 2560 x 1920 that was used for image acquisition and the exposure time was set to auto-exposure. The "auto-white" balance option via camera settings was set on a clear area of the slide. The images were captured at a scaling per pixel (px) of 0.48 (µm/px) and saved as a Tagged Image File Format (TIFF). Three images per slide were captured for the duodenal, jejunal, ileal and colon segments, however, only images from the ileum and colon segments were used for image analysis because the duodenum and jejunum segments were too digested (autolysed) **(Figure 6.1)** preventing measurements of intact villi.

3.4.2. Image analysis

The open-source software, FIJI (Schindelin *et al.*, 2012) **(Table 6.1)** was used for image analysis. Firstly, the set scale option from the "Analyse" tab was selected and the scale was set to 2.0833 pixels/µm using the scaling per pixel value of 0.48 µm/px. The segmented line tool was selected for measuring villus length (µm) in the ileum and crypt depth (µm) in the colon from images of both MD (n=3) and HFD (n=6) groups. The average villus length and crypt depth for each group was calculated and the data were represented as villus length/ crypt depth (µm) ± SD.

Ileum	Colon
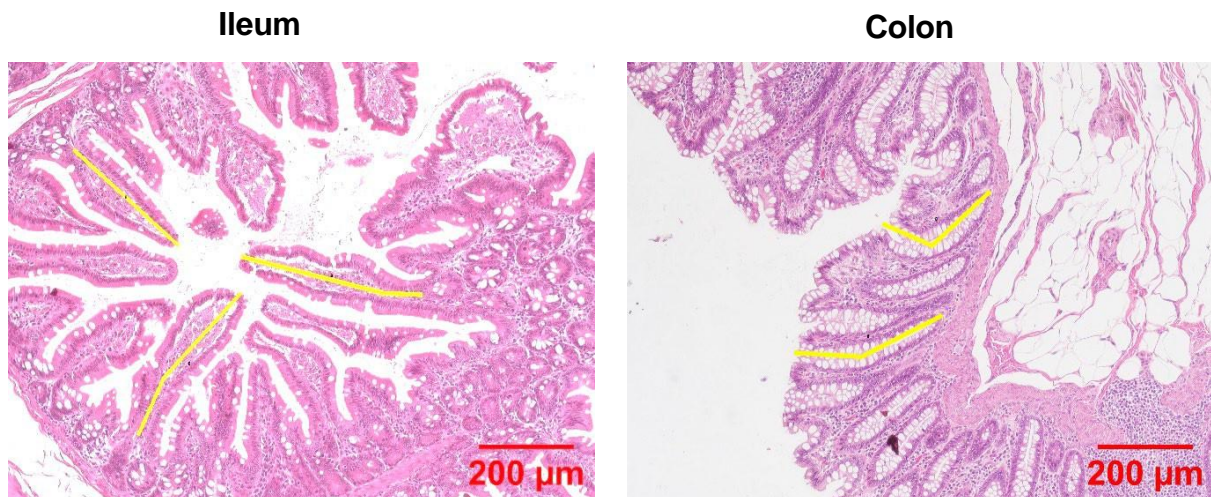
Figure 3.2: Morphometric analysis using haematoxylin and Eosin-stained images. Representative images depicting the morphology of the ileum **(A)** and colon **(B)** of vervet monkeys. A yellow segmented line was used to measure the length (µm) of intact villi in the ileum (n=3) and crypt depth (µm) in the colon (n=2) using an open source software, FIJI.

3.5. Investigation of intestinal barrier function and intestinal immunity using immunohistochemistry

Immunohistochemistry (IHC) is a technique that relies on the binding of an antibody to the cellular or tissue antigen of interest and the antibody binding to the tissue antigen is then detected by a secondary antibody complex labelled by a chromogen or fluorophore detectable by a microscope (Katikireddy and O'Sullivan, 2011). IHC was used to assess the expression of the intestinal barrier function marker, (occludin) and the population of plasma cells (IgA$^+$ cells) (intestinal immunity marker) in formalin-fixed intestinal sections of vervet monkeys. The tissue slides were dewaxed and dehydrated **as described in 3.4**.

3.5.1. Antigen retrieval

To optimise the detection of the antigens of interest, tissue slides with and without antigen retrieval were tested. Compared to tissue slides without antigen retrieval, antigen detection was enhanced following antigen retrieval, as such, heat-induced epitope retrieval, was applied for all tissue slides for the detection of occludin and IgA$^+$ cells. Slides immersed in 0.01 M citrate buffer (pH 6.0) **(Table 6.2)** were incubated at 125ºC for 30 seconds and 90ºC for 10 seconds in a DakoCytomation Pascal Pressure Chamber **(Table 6.1)** along with PASCAL Paper Strips for quality control. Following

incubation, the tissue slides were allowed to cool down in the buffer at room temperature for 20 minutes. Slides were rinsed in distilled water for five minutes in a staining jar with a stir bar.

3.5.2. Blocking and antibody incubation

The slides were rinsed in 0.05 M Tris-buffered saline (TBS) pH 7.2 and 0.5% triton X-100 (TBS-triton) **(Table 6.3)** for five minutes in a staining jar. Then, 150 µL of normal donkey serum (1:20 in PBS) **(Table 6.3)** was added to the sections in a moisture chamber for 30 minutes at room temperature. The primary antibodies were diluted in 0.1 M PBS pH 7.2 with 0.01% of sodium azide and 0.1% of bovine serum albumin (BSA) **(Table 6.3)**. The slides were incubated with the respective primary antibodies in a moisture chamber using optimised dilutions **(Table 3.1)** overnight at 4ºC. The slides were equilibrated to room temperature for 30 minutes before being jet washed and rinsed for five minutes in a staining jar with TBS-triton. The secondary antibody, Dylight 488 **(Table 6.2)** was added at optimised dilutions **(Table 3.1)** (1:800) in PBS with sodium azide) onto the slides and then incubated for one hour in the dark at room temperature.

Table 3.1: List of antibodies (primary and secondary) and serum used for immunohistochemical analysis of intestinal tissues in vervet monkeys (*Chlorocebus aethiops*)

Primary Antibody	Primary Antibody Dilution	Secondary Antibody (1:800)	Serum (1:20)
Mouse IgA antibody #NBP2-61794	1:500	Donkey anti-Mouse (Dylight 488) #715-545-150	Normal donkey serum
Mouse occludin monoclonal antibody #33-1500	1:500	Donkey anti-mouse (Dylight 488) #715-545-150	Normal donkey serum

The slides were jet washed and rinsed in TBS-triton for five minutes in a staining jar. The slides were rinsed in 0.05 M TBS pH 7.2 **(Table 6.3)** for five minutes. Thereafter, 150 µL of Hoechst 33342 stain **(Table 6.2)** (1 µg/mL) diluted in TBS was added to each slide and incubated for 10 minutes in a moisture chamber in the dark to stain the nuclei. The slides were jet washed and rinsed in TBS-triton for five minutes in a

staining jar. Slides were rinsed in a staining jar with distilled water for five minutes, mounted onto coverslips with Dako anti-fade mounting medium **(Table 6.2)** and stored in the dark at room temperature for one hour in preparation for imaging.

3.5.3. Widefield fluorescence microscopy – imaging IgA$^+$ tissue area

Widefield fluorescence microscopy is an imaging technique that uses light of a specific wavelength to illuminate and excite molecules (fluorophores) of a sample. The excited fluorophores emit light that is then passed through an emission filter which transmits light to the camera to be imaged (Dunst and Tomancak, 2019). Hoechst 33342 stained regions were visualised as nuclei-positive regions using the blue channel. Dylight 488 **(Table 6.2)** stained regions were visualised as IgA$^+$ cells using the green channel on the Nikon Eclipse Ti-inverted microscope. Hoechst 33342 has a peak excitation wavelength of 350 nm and an emission wavelength of 461 nm. Dylight 488 has a peak excitation wavelength of 492 nm and an emission wavelength of 519 nm. Images were acquired using a Nikon Plan Apo 10x objective and a Nikon DS-Fi1c camera. Using the NIS-Elements software, a multi-channel stack image per slide was acquired (Acquisition> Scan large image) at a scaling per pixel of 0.48 (µm/px). The images from both the blue and green channels were captured and stitched via the "Blending" option with a 15% overlap between the images to generate a single file (multi-channel stack image). Images of the blue channel represented the nuclei-stained regions whereas the green channel images represented IgA$^+$-cells-stained regions. Stacks acquired from the duodenum, jejunum, ileum and colon were used to quantify IgA$^+$ tissue area.

3.5.4. Image analysis for IgA$^+$ tissue area

FIJI was used to quantitate the percentage positive area of IgA$^+$ cells in the duodenum, jejunum, ileum and colon. In each multi-channel stack, images of the blue channel were removed and the image of the green channel was used for analysis. The scaling per pixel value of 0.48 (µm/px) of the images was used to set the scale to 2.0833 pixels/µm (Analyse> set scale) and the images converted to 8-bit TIFF format (Image> type> 8 bit). For each image, regions of interest (ROIs) were drawn around a tissue area with IgA$^+$ cells **(Figure 3.2)**. Manual thresholding (Image> adjust> threshold) was utilised to create a binary image and a mask was created (Process> binary> convert to mask) **(Figure 3.2)**. The area positive for IgA$^+$ cells (µm²) within ROIs of the mask images was measured by analysing particles (Analyse> analyse particles). The total

area of tissue (μm²) within the ROIs was measured (Analyse> measure). The formula below was used to calculate the percentage area of IgA$^+$ cells. The data were represented as % positive area ± SD.

$$\% \ Positive \ area = \frac{IgA^+ \ area \ (\mu m^2)}{Total \ area \ of \ ROIs \ (\mu m^2)} * 100$$
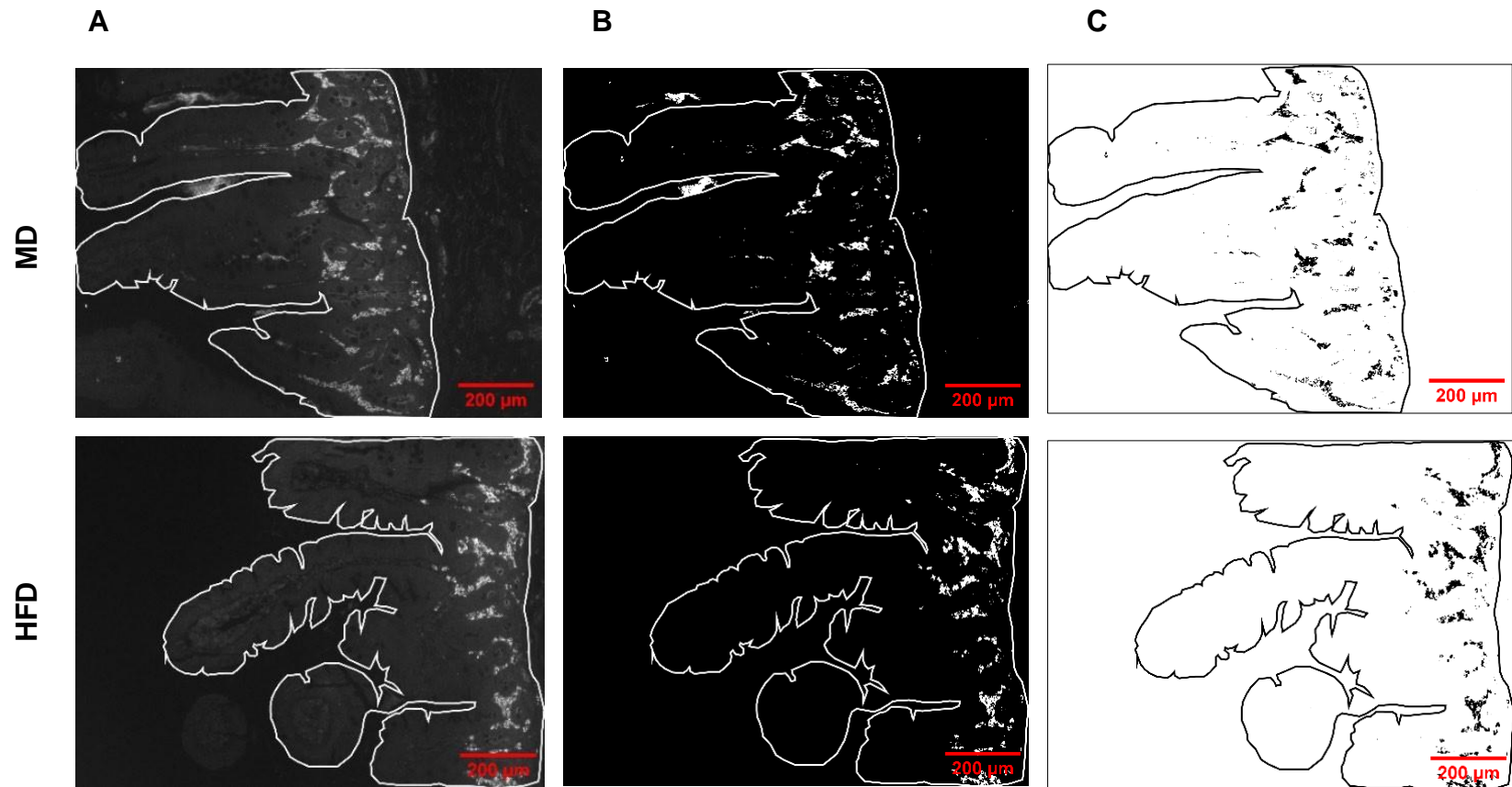
Figure 3.3: Analysis of images depicting intestinal IgA$^+$ cells of MD-fed and HFD-fed vervet monkeys (*Chlorocebus aethiops*). Intestinal-tissue-area positive for IgA expressing cells (grey **(A)**, white **(B)**, and black **(C)** particles) for both MD-fed and HFD-fed vervet monkeys. Manual thresholding was used to create a binary image **(B)** from which a "mask" image was created to analyse particles (area positive for IgA$^+$ cells) within the drawn regions of interest **(C)**. Abbreviations: maize-based diet (MD) and high-fat diet (HFD).

3.5.5. Confocal laser scanning microscopy – imaging occludin expression

Confocal laser scanning microscopy is an imaging technique that utilises a laser light source that is filtered through a pinhole to enable only in-focus light to reach the specimen, blocking out-of-focus light. The emitted light is visualised through an eyepiece or captured by a camera (Shah *et al.*, 2022). For image acquisition, a Carl Zeiss LSM78 with ELYRA PS1 confocal microscope **(Table 6.1)** equipped with a Plan Apochromat 20x/0.8 M27 objective and a Plan-Apochromat 63x/1.4 Oil DIC objective, was used on the ZEN 2012 imaging software **(Table 6.1)**. Two channels were used for image acquisition, Hoechst 33342 (blue channel) and Dylight 488 (green channel). The Plan Apochromat 20x/0.8 M27 objective was used to capture a 3x3 tile scan image and a snapshot image. A region of interest (ROI) from the snapshot image was then selected to acquire a z-stack image using the Plan-Apochromat 63x/1.4 Oil DIC objective. Two z-stack images acquired per slide from the ileum and colon were used to quantify the mean fluorescence intensity of occludin.

3.5.6. Image analysis for occludin expression

FIJI was used for quantification of occludin fluorescence intensity in the ileum and colon of monkeys using z-stack images acquired with the Plan-Apochromat 63x/1.4 Oil DIC objective. The z-stack images were saved in czi format using the ZEN 2012 imaging software. The czi file was opened with FIJI as hyperstack and an option of "split channels" was selected. The Hoechst 33342 channel z-stack image was excluded from analysis, and the Dylight 488 z-stack image was used for further analysis. A single 8-bit image was generated (Image> Z project> sum slices), to quantify mean grey values, (Analyse> set measurements and tick the "Mean grey value" and click "Ok") (Willett, 2019). Thereafter, the image was saved in TIFF format, ROIs positive for occludin were drawn **(Figure 3.3)** and the mean grey value was calculated (Analyse> Measure) in each ROI and the background of each image. The background mean grey value of each image was subtracted from the mean grey value of each ROI (Process> Math> Subtract and input the mean grey value) of that image. This procedure was done for all z-stack images acquired from the ileum and colon. The data were represented as mean fluorescence intensity (mean grey values) ± SD.
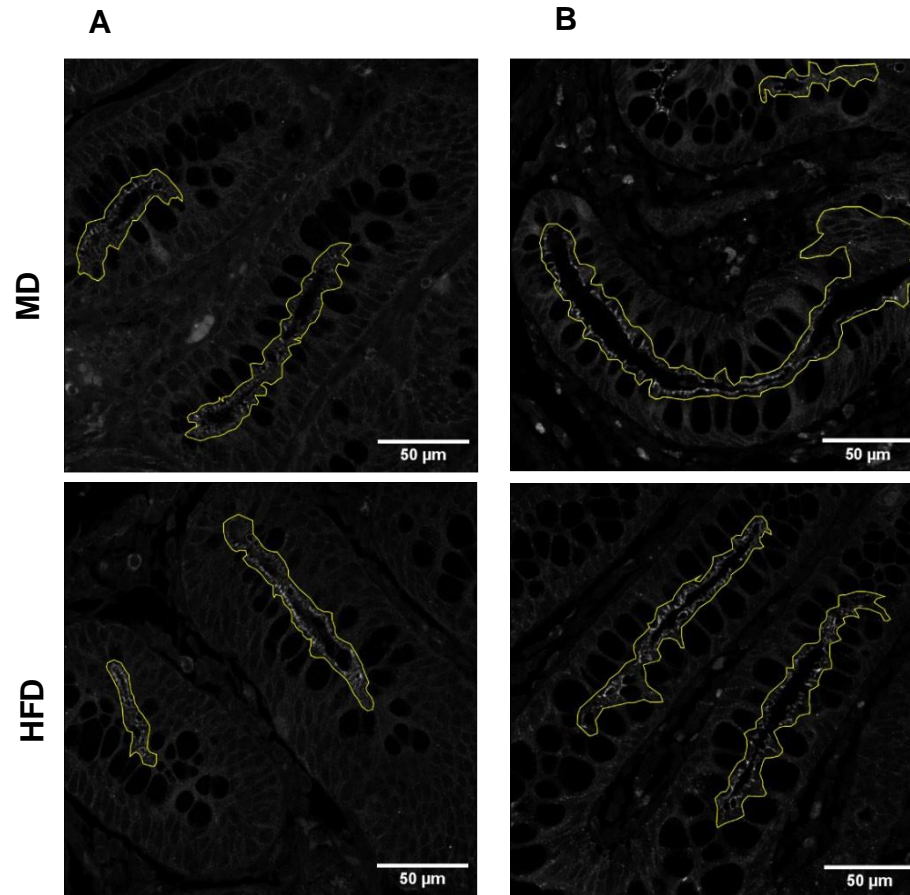
Figure 3.4: Analysis of images depicting the expression of intestinal occludin in MD-fed and HFD-fed vervet monkeys (*Chlorocebus aethiops*). Occludin-stained regions (polygon shapes) in the ileum **(A)** and colon **(B)** of MD-fed and HFD-fed vervet monkeys. Abbreviations: maize-based diet (MD) and high-fat diet (HFD).

3.6. Investigation of intestinal tissue proteins expression using western blot

Western blot is a technique that detects protein(s) of interest within a sample with the use of a probe such as an antibody. It is based on the separation of the proteins on size using polyacrylamide gel electrophoresis, followed by the transfer of the separated proteins onto a membrane. Thereafter, the antibodies are loaded onto the membrane for the detection of the target protein(s) (Nicholas and Nelson, 2013).

3.6.1. Protein isolation

Due to autolysis of duodenum and jejunum tissue sections as described in **section 3.4.1**, these sections were excluded from western blot analysis. Between 50-100 mg of tissue from the ileum (n=8) and colon (n=8) of vervet monkeys was weighed and placed in microcentrifuge tubes. An appropriate volume (10 µL of cell-lysis buffer per 1 mg of tissue) of cell-lysis buffer **(Table 6.3)** was added to the samples along with a stainless-steel ball. The tubes were homogenised using a Qiagen MM300 Mixer Tissue Lyser **(Table 6.1)** at 25 Hertz for 60 seconds whereafter the samples were cooled on ice for 60 seconds: this step was repeated four times. The tubes were centrifuged for 15 minutes (17,135 x g) at 4ºC and the supernatant (tissue lysate) was carefully transferred to fresh tubes and placed on ice or stored at -80ºC.

3.6.2. Protein quantification

The protein concentration of the tissue lysates was determined using the Bio-Rad DC Protein assay **(Table 6.2)**. Similar to the Lowry assay, the reaction between the protein and the alkaline copper tartrate followed by the reduction of the Folin reagent by the copper-treated protein leads to colour development. The reaction is characterised by the formation of a blue colour with a maximum absorbance at 750 nm that can be measured using a spectrophotometer (Peterson, 1979). To determine the protein concentration, 5 µL of the BSA standards (0.125, 0.25, 0.5, 0.75, 1.0, 1.5, and 2 mg/mL) and 5 µL of each diluted sample (1:10 in PBS) (prepared in duplicates) were added to wells in a 96-well plate. Subsequently, reagent A' was prepared by adding 20 µL of reagent S to each 1 mL of reagent A, and 25 µL of reagent A' was then added to the wells followed by 200 µL of reagent B. After 15 minutes of incubation at room temperature, the absorbance was measured at 750 nm using the Spectramax i3 multimode plate reader **(Table 6.1)**, and the absorbance values of the standards were used to construct a standard curve to calculate the amount of protein (µg/mL) in each sample.

3.6.3. Sodium dodecyl sulphate polyacrylamide gel electrophoresis

After protein determination, protein samples were diluted in 2X Laemli sample buffer **(Table 6.2)**, incubated for five minutes at 95ºC and placed on ice. The gels were prepared by following the 12% TGX Stain-Free FastCast kit gel **(Table 6.2)** recipe calculator. To prepare the resolving gel, 3 mL of resolvers A and B were added to a fresh tube. Then, 3 µL of N, N, N', N' Tetramethylethylene-1,2-diamine (TEMED) **(Table 6.2)** and 30 µL of 10% ammonium persulphate (APS) **(Table 6.2)** were added to the resolver A and B solution. The solution was then transferred to 1.0 mm Bio-Rad glass plates assembled in a casting chamber. To prepare the stacking gel, 1 mL of stackers A and B were added to a fresh tube. Then, 2 µL TEMED and 10 µL of 10% (APS) were added to the stacker A and B solution. The solution was then transferred to the 1.0 mm Bio-Rad Glass Plates with the resolving gel. The gels were allowed to polymerise for 45 minutes at room temperature with 10-well combs inserted between the plates. Polymerised gels were placed in a Mini-PROTEAN Tetra Cell **(Table 6.1)** filled with 1x Running buffer **(Table 6.3)**. Subsequently, 5 µL of Precision Plus Protein WesternC molecular marker **(Table 6.2)** and 30 µg of protein per well was loaded for each sample onto the gel. Finally, proteins were separated at 100 V for 10 minutes, followed by 120 V for 60 minutes. The stain-free gel was exposed to UV light for 45 seconds on the ChemiDoc MP imaging system **(Table 6.1)** to enable activation of the trihalo compounds in the stain-free gel that bind to the proteins in the gel and facilitate total protein detection after the transfer.

3.6.4. Transfer of proteins to polyvinylidene fluoride membrane

The polyvinylidene fluoride (PVDF) membrane **(Table 6.2)** was activated by gently shaking in 100% methanol **(Table 6.2)** for two minutes, followed by gently shaking in distilled water for five minutes. Thereafter, the PVDF membrane along with the cut Whatman papers, fibre pads and gels were equilibrated by gently shaking in the transfer buffer **(Table 6.3)** for 20 minutes. The wet transfer method was used for the transfer of proteins from the sodium dodecyl-sulfate polyacrylamide gel electrophoresis gel onto an activated PVDF membrane using the Mini Trans-Blot Cell **(Table 6.1)**. Firstly, a 'sandwich' was assembled by opening the cassette, placing the black (negative) side down, and a fibre pad followed by Whatman papers, gel, PVDF membrane, Whatman papers, and fibre pad. The cassette was placed between the electrodes, an ice pack was then placed in the tank filled with transfer buffer, followed

by transfer at 160 V for 75 minutes at 4ºC. A stain-free blot of the PVDF membranes was imaged using the ChemiDoc MP imaging system **(Table 6.1)** for total protein measurement in each lane.

3.6.5. Primary and secondary antibodies

The PVDF membranes were blocked for non-specific binding in Tris-buffered saline with Tween 20 (TBST) **(Table 6.3)** containing 5% non-fat milk for two hours on a shaker. This was followed by rinsing with TBST twice prior to incubation with the respective diluted primary antibodies in TBST **(Table 3.2)** at 4ºC on a shaker overnight. The following day, the membranes were washed three times for 10 minutes in TBST. The membranes were then incubated with the corresponding secondary antibodies diluted **(Table 3.2)** in 2.5% non-fat milk in TBST (20 mL) along with 2 µL of Precision Protein StrepTactin-Horseradish peroxidase (HRP) Conjugate **(Table 6.2)** for detection of the molecular marker at room temperature for two hours. After incubation, the membranes were washed three times for 10 minutes in TBST for chemiluminescence detection.

Table 3.2: List of primary and secondary antibodies used for western blots

Primary Antibody	Molecular Weight (kDa)	Primary Antibody Dilution	Secondary Antibody (1:4000)
Total p44/42 MAPK (ERK1/2) (137F5) rabbit mAb #4695	42, 44	1:1000	Anti-rabbit IgG, HRP-linked antibody #7074
Phospho-p44/42 MAPK (ERK1/2) (Thr202/Tyr204) rabbit mAb #9101	42, 44	1:1000	Anti-rabbit IgG, HRP-linked antibody #7074
Total p38 MAPK (D13E1) XP® rabbit mAb #8690	38	1:1000	Anti-rabbit IgG, HRP-linked antibody #7074

3.6.6. Chemiluminescent detection and image analysis

The Chemiluminescent Substrate Kit **(Table 6.2)** was used for detection the of bound proteins on the membrane. Equal parts of solution A (2 mL) and B (2 mL) were mixed for incubation with the membrane for five minutes on a shaker, then the membrane was imaged on the ChemiDoc MP imaging system. Image Lab (version 6.1.0 build 7) **(Table 6.1)** was used for normalisation and to generate densitometric data of chemiluminescence images depicting the target protein with respective total protein

images. The phosphorylation of ERK1/2 (expression of ERK1/2) was calculated using the formula below and represented as phosphorylated/ total ERK ± SD. The expression of p38 was represented as fold change ± SD.

$$Phosphorylation/\ Expression\ ERK = \frac{Phosphorylated\ ERK1/2}{Total\ ERK1/2}$$

3.7. Assessment of systemic parameters of intestinal barrier function and inflammation using enzyme-linked immunosorbent assay

3.7.1. Lipopolysaccharide-binding protein detection using enzyme-linked immunosorbent assay

Lipopolysaccharide-binding protein (LBP) kit **(Table 6.2)** was used for the detection of LBP in the serum of vervet monkeys, and it is based on the sandwich-ELISA principle which relies on the binding of an antigen of interest to the capture antibody. The bound antigen is then "sandwiched" or bound with a secondary antibody conjugated to an enzyme. A substrate solution is then added to produce a colour change that indicates reactivity between the capture antibody and antigen (Wilson and Walker, 2010).

3.7.1.1. Reagent and sample preparation

Reagents supplied in the kit were equilibrated to room temperature before use. A 1X wash buffer was prepared from a 25X stock solution by diluting it with distilled water **(Table 6.2)**. Biotinylated detection antibody solution (100X) and HRP conjugate solution (100X) was diluted with their respective diluents, to yield 1X working solutions **(Table 6.3)**. Serum samples (n=9) were diluted (1:10) at tested optimised dilutions with the sample diluent to yield working serum solutions. To prepare the standard working solution (20 ng/mL), 1 mL of the reference standard and sample diluent was added to the standard tube and then inverted gently after 10 minutes. Serial dilutions were made following the dilution gradient: 20, 10, 5, 2.5, 1.25, 0.63, and 0.31 ng/mL as described in the kit. The reference standard and sample diluent were used as a blank.

3.7.1.2. Assay procedure

The 96-well ELISA plate supplied in the kit was pipetted with 100 μL of the standards (20, 10, 5, 2.5, 1.25, 0.63, 0.31 ng/mL), serum samples (1:10) and blank (0 ng/mL) in duplicates, and the plate was incubated for 90 minutes at 37ºC. Sample and standard

solutions were discarded by inverting onto a paper towel and 100 µL of 1X Biotinylated detection antibody was added to wells of the plate and incubated for one hour at 37ºC. The solution was discarded, and the plate was washed three times with 1X wash buffer (350 µL per well) for one minute. Thereafter, 100 µL of 1X HRP conjugate was added to wells and the plate was incubated for 30 minutes at 37°C. The solution was discarded, and the plate was washed five times for two minutes. Following this, 90 µL of the substrate reagent was added to the wells and incubated for 15 minutes at 37°C. Following incubation, 50 µL of the stop solution was added and the absorbance was measured at 450 nm using Spectramax i3 multimode plate reader. A four-parameter logistic curve fit was used to determine the sample concentration (ng/mL) from the absorbance values of the samples and the concentration values were adjusted for sample dilution by multiplying them by 10. The data were represented as mean concentration (ng/mL) ± SD.

3.7.2. Cluster of differentiation 14 detection using Enzyme-Linked Immunosorbent Assay

3.7.2.1. Reagent and sample preparation

Cluster of differentiation 14 (CD14) kit **(Table 6.2)** was used for the detection of CD14 in serum. The reagents supplied in the kit were equilibrated to room temperature prior to use. A 1X solution of assay diluent was prepared from a 5X stock solution of assay diluent and 1X wash buffer was prepared from a 20X stock solution by diluting with distilled water **(Table 6.3)**. A vial of Biotinylated detection antibody was reconstituted with 100 µL of 1X assay diluent to make an 80X stock solution of Biotin conjugate, which was used to prepare a 1X working solution **(Table 6.3)**. Streptavidin-HRP conjugate solution (600X) was diluted with 1X assay diluent to yield 1X working solution **(Table 6.3)**. Serum samples (n=9) were diluted (1:100) with the 1X assay diluent at tested optimised dilutions to yield working serum solutions. To prepare the standard working solution (50 ng/mL), 800 µL of 1X assay diluent was added to the reference standard vial and gently mixed by pipetting up and down. Serial dilutions were made following the dilution gradient: 50, 20, 8, 3.200, 1.280, 0.512, 0.205 ng/mL as described in the kit. The CD14 standard and assay diluent were used as a blank.

3.7.2.2. Assay procedure

The 96-well ELISA plate was pipetted with 100 µL of the standards (50, 20, 8, 3.200, 1.280, 0.512, 0.205 ng/mL), serum samples (1:100) and blank (0 ng/mL) in duplicates. The plate was incubated for two hours and 30 minutes at room temperature on a plate shaker **(Table 6.1)** at 500 rpm. The liquid was discarded by inverting onto a paper towel and the plate was washed four times (300 µL per well) with 1X wash buffer. After the fourth wash, the buffer was discarded and 100 µL of 1X Biotin conjugate solution was added to each well. The plate was incubated for 60 minutes at room temperature on a plate shaker. The solution was then discarded, and the plate was washed four times with 1X wash buffer as described above, and after discarding the washing solution, 100 µL of Streptavidin-HRP solution was added to each well. The plate was incubated for 45 minutes at room temperature on a plate shaker and the solution was discarded and the plate was washed four times with 1X wash buffer (300 µL per well). TMB substrate solution was added (100 µL) to each well, and the plate was incubated for 30 minutes at room temperature in the dark on a plate shaker. Following incubation, 50 µL of the stop solution was added and the absorbance was measured at 450 nm using Spectramax i3 multimode plate reader. A four-parameter logistic curve fit was used to determine the sample concentration (ng/mL) from the absorbance values (nm) of the samples and the concentration values were adjusted for sample dilution by multiplying them by 10. The data were represented as concentration mean (ng/mL) ± SD.

3.8. Statistical analysis

The data were represented as mean ± SD. The data were tested for normality by Kolmogorov-Smirnov's test and statistical differences between the MD and HFD were calculated using GraphPad Prism 8 for Windows Version 8.4.2 software **(Table 6.1)** by unpaired t-tests with Welch's correction. A p-value $p \leq 0.05$ was considered significant and $p \leq 0.1$ was considered marginally significant.

CHAPTER FOUR

4. Results

4.1. The effect of a high-fat diet on glycaemic and lipid parameters

There were no significant differences (p=0.237) in FBG levels (mmol/L) and HbA1c levels (p=0.342) between the HFD-fed and MD-fed monkeys **(Table 4.1)**. Furthermore, there were no significant changes in triglyceride levels (p=0.813) between the HFD-fed and MD-fed monkeys. However, there was a slight increase in cholesterol levels (p=0.071) and a significant increase in HDL-C (p=0.048) and LDL-C (p=0.017) levels (mmol/L) in HFD-fed monkeys when compared to the MD-fed monkeys **(Table 4.1).**

Table 4.1: Glycaemic and lipogram parameters of MD-fed and HFD-fed vervet monkeys (*Chlorocebus aethiops*)

Measurement	Diet group		p
	MD	**HFD**	
Fasting glucose (mmol/L)	4.30 ± 0.17	4.82 ± 0.92	0.237
HbA1c (%)	4.23 ± 0.12	4.40 ± 0.36	0.342
Triglyceride (mmol/L)	1.21 ± 0.63	1.33 ± 0.71	0.813
Total cholesterol (mmol/L)	3.83 ± 2.34	7.97 ± 1.64	**0.071**
HDL-C (mmol/L)	1.70 ± 0.87	4.45 ± 2.50	**0.048**
LDL-C (mmol/L)	1.73 ± 1.40	5.52 ± 1.93	**0.017**

All data are represented as mean ± SD, n=9. Abbreviations: maize-based diet (MD), high-fat diet (HFD), glycated haemoglobin (HbA1c), low-density lipoprotein cholesterol (LDL-C) and high-density lipoprotein cholesterol (HDL-C).

4.2. The effect of a high-fat diet on intestinal morphology

Morphological changes in the ileum and colon vervet monkeys were assessed by H&E staining. As described in **section 3.4.1,** the duodenum and jejunum sections were excluded from analysis. Representative images depicting the morphology of the ileum and colon are shown in **Figure 4.1**. FIJI was used to measure the villus length (μm) in the ileum and crypt depth (μm) in the colon of both MD-fed and HFD-fed monkeys. It was evident that there were no significant differences in both villus length (p=0.185) and crypt depth (p=0.522) between HFD-fed and MD-fed vervet monkeys **Figure 4.1B, C**.
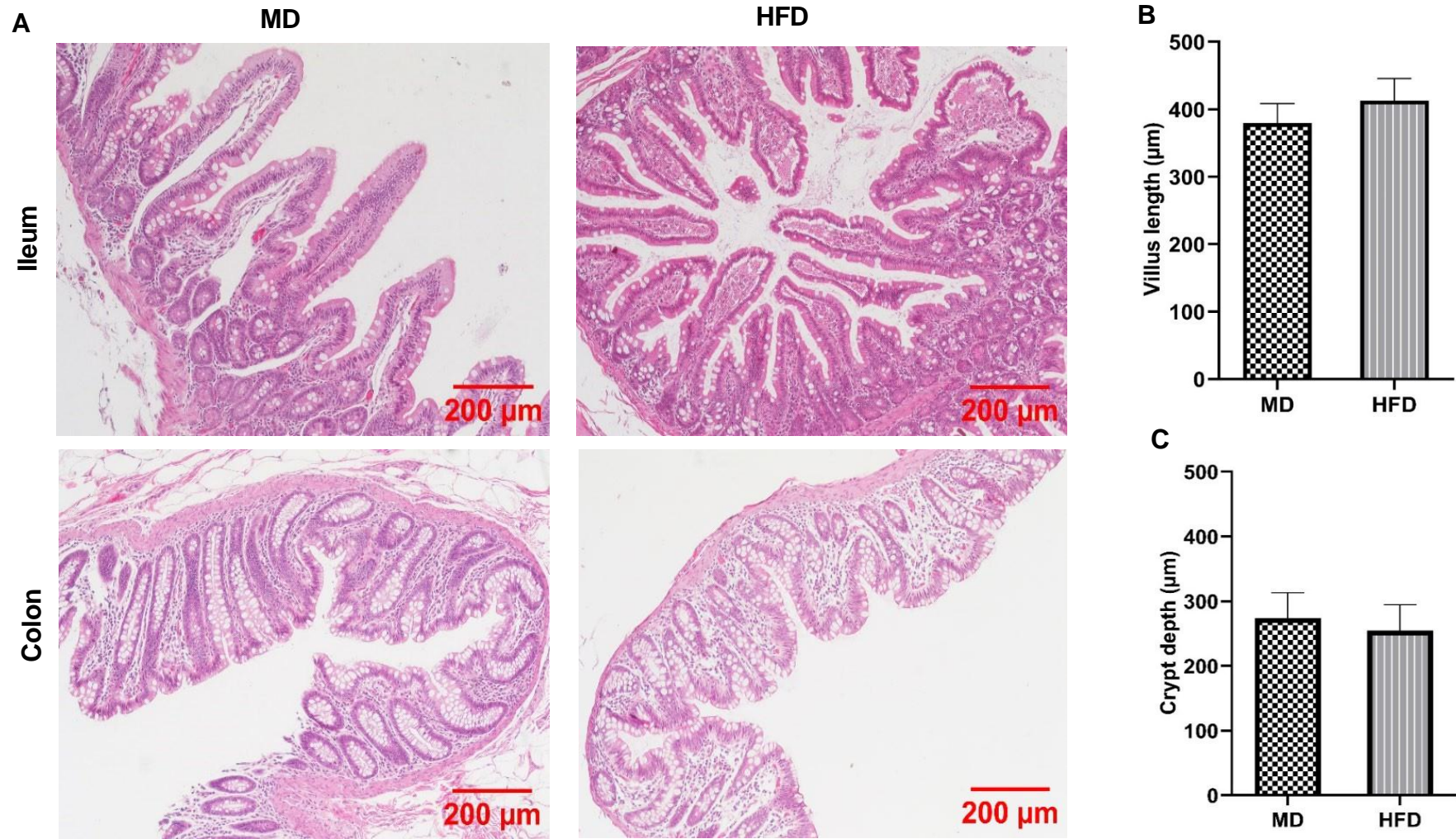
Figure 4.1: The effect of an HFD on intestinal morphology of vervet monkeys (*Chlorocebus aethiops*). Representative images depicting the morphology of the ileum and colon of the MD-fed and HFD-fed vervet monkeys **(A)**. The length (µm) of the villus in the ileum **(B)** and crypt depth (µm) in the colon **(C)** of both the MD-fed and HFD-fed monkeys. All data are represented as mean ± SD, n=9. Abbreviations: maize-based diet (MD) and high-fat diet (HFD)

4.3. The effect of a high-fat diet on intestinal plasma cells- IgA$^+$ cells

The effect of an HFD on the population of IgA$^+$ cells in the duodenum, jejunum, ileum and colon of vervet monkeys was detected by IHC. FIJI was used to quantify the % positive area of IgA$^+$ cells. Representative images depicting IgA$^+$ cells in the duodenum, jejunum, ileum and colon of both HFD-fed and MD-fed monkeys were acquired using wide-fluorescence microscopy are shown in **(Figure 4.2)**. As shown in **Figure 4.3A**, the % positive area in the duodenum of the HFD-fed monkeys was significantly higher (p=0.046) when compared to the MD-fed monkeys. However, there were no significant differences between the % positive area of the jejunum, ileum and colon of the HFD-fed and MD-fed monkeys **(Figure 4.3B, C, D)**.
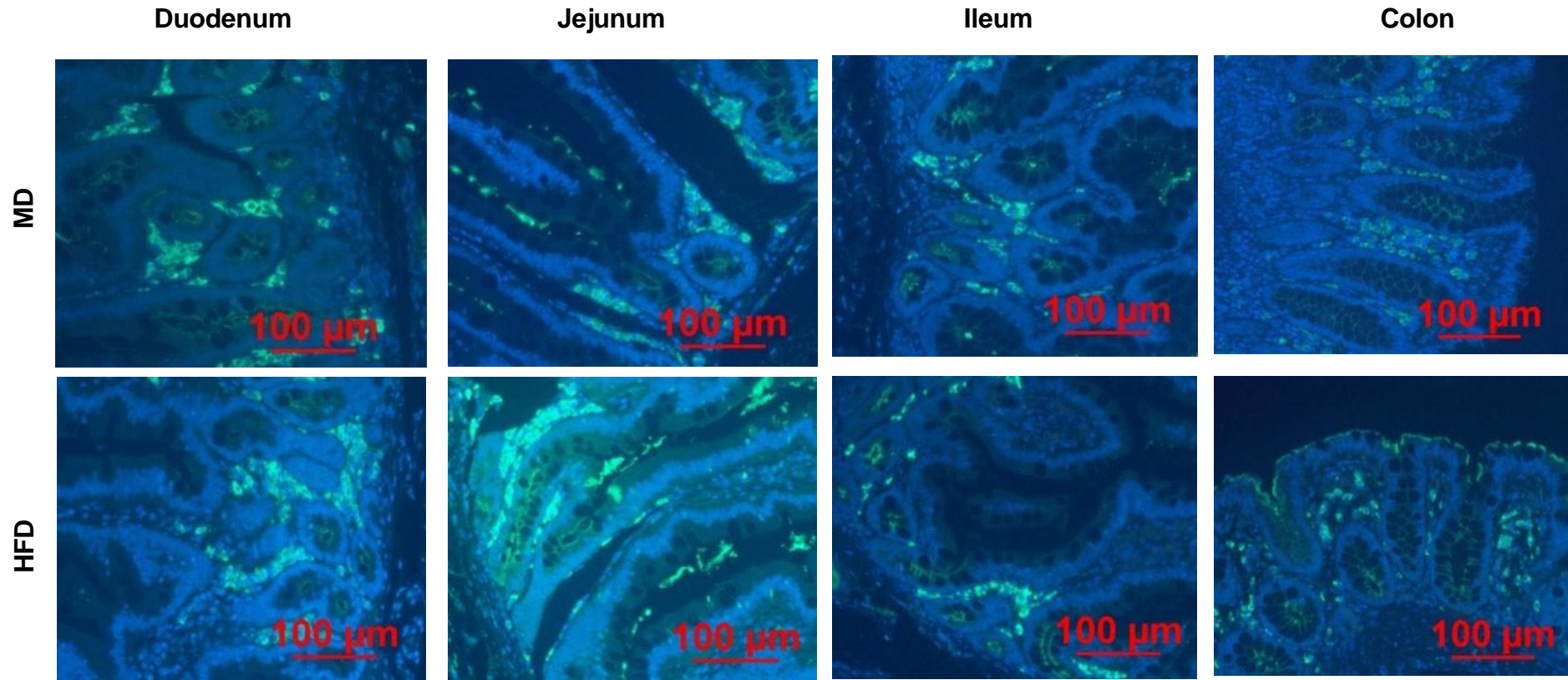
Figure 4.2: The effect of an HFD on the intestinal population of IgA$^+$ cells in vervet monkeys (*Chlorocebus aethiops*). Representative merged images of the presence of IgA$^+$ cells in the duodenum, jejunum, ileum and colon of MD-fed and HFD-fed vervet monkeys were acquired using wide-fluorescence microscopy. Hoechst 33342 stained regions were visualised as nuclei-positive regions using the blue channel. Dylight 488 stained regions were visualised as IgA+ cells using the green channel on the Nikon Eclipse Ti-inverted microscope. Abbreviations: maize-based diet (MD) and high-fat diet (HFD).
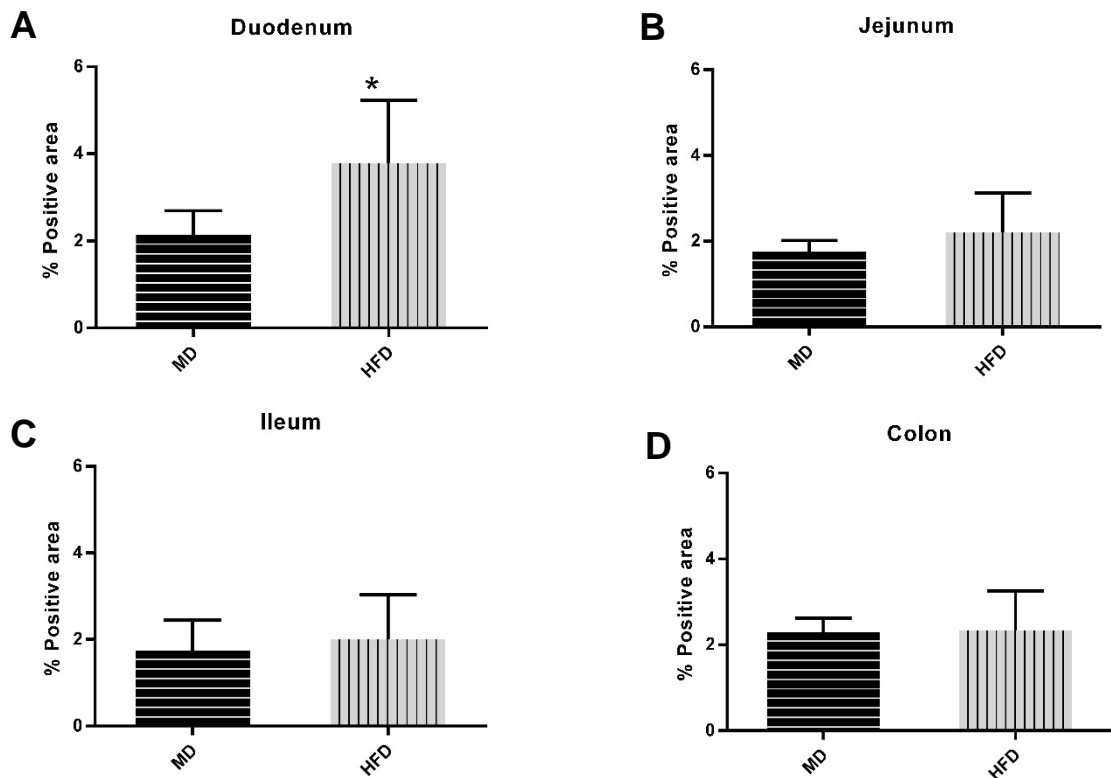
Figure 4.3: The effect of an HFD on the intestinal population of IgA$^+$ cells in vervet monkeys (*Chlorocebus aethiops*). The population of IgA$^+$ cells are represented as % positive area in the duodenum **(A)**, jejunum **(B)**, ileum **(C)** and colon **(D)** of both HFD-fed and MD-fed vervet monkeys. All data are represented as mean ± SD, n=9. Abbreviations: maize-based diet (MD) and high-fat diet (HFD). (* p ≤ 0.05).

4.4. The effect of a high-fat diet on expression of occludin in the intestinal tissues

IHC was used to detect the expression of occludin, which was quantified as mean grey values using FIJI and represented as mean fluorescence intensity. Representative images depicting the expression of occludin in the ileum and colon of both HFD-fed and MD-fed monkeys acquired using confocal microscopy are shown in **(Figure 4.4A)**. There were no significant differences in the expression of occludin in the ileum (p=0.902) and colon (p=0.541) between the HFD-fed and MD-fed groups **(Figure 4.4B, C)**.
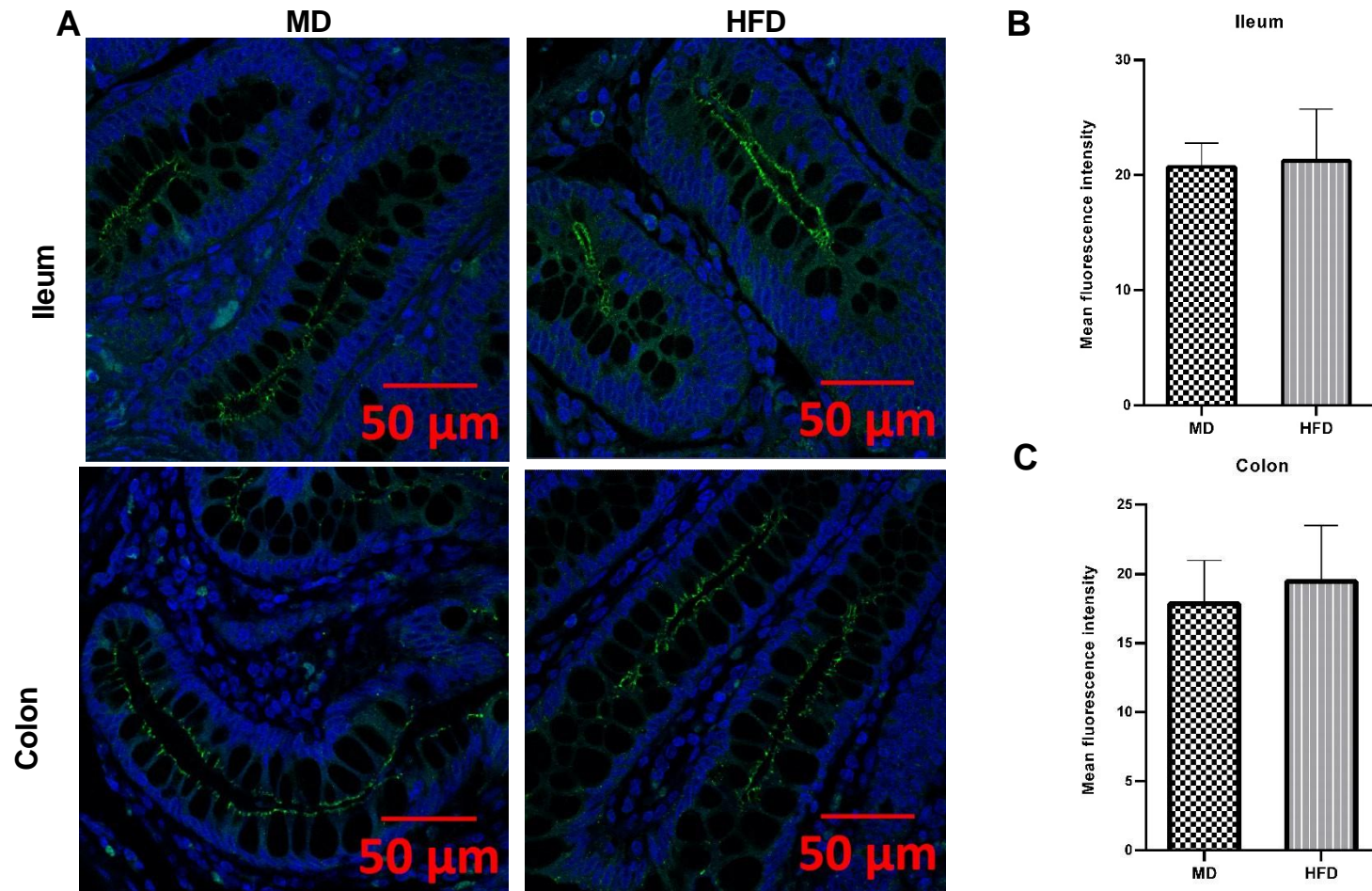
Figure 4.4: The expression of occludin in the ileum and colon of vervet monkeys (*Chlorocebus aethiops*). Representative merged images depicting the expression of occludin in the ileum and colon of both MD-fed and HFD-fed vervet monkeys were acquired using confocal microscopy **(A)**. The expression of occludin was represented as mean fluorescence intensity in the ileum **(B)** and colon **(C)** of both the HFD-fed and MD-fed vervet monkeys. All data are represented as mean ± SD, n=9. Abbreviations: maize-based diet (MD) and high-fat diet (HFD). (* p ≤ 0.05)

4.5. The effect of a high-fat diet on intestinal expression of pro-inflammatory mediators

Antibodies specific for intestinal inflammation markers were assessed using western blot analysis. Unfortunately, none of them were detectable **(Table 6.5)**. However, the expression of MAPKs which play a role in the synthesis of pro-inflammatory mediators, ERK1/2 and p38, (Liu and Zhu, 2022) were quantified using Image Lab software. Chemiluminescence images depicting bands indicative of the presence of phosphorylated ERK (pERK) and total ERK (tERK) in the ileum and colon of vervet monkeys **(Figure 4.5A, B)**. Phosphorylation of ERK1/2 was represented as the ratio of phosphorylated to total ERK 1/2. There were no significant differences in phosphorylation of ERK1/2 between MD-fed and HFD-fed monkeys in the ileum (p=0.322) and colon (p=0.134) **(Figure 4.5C, D)**.
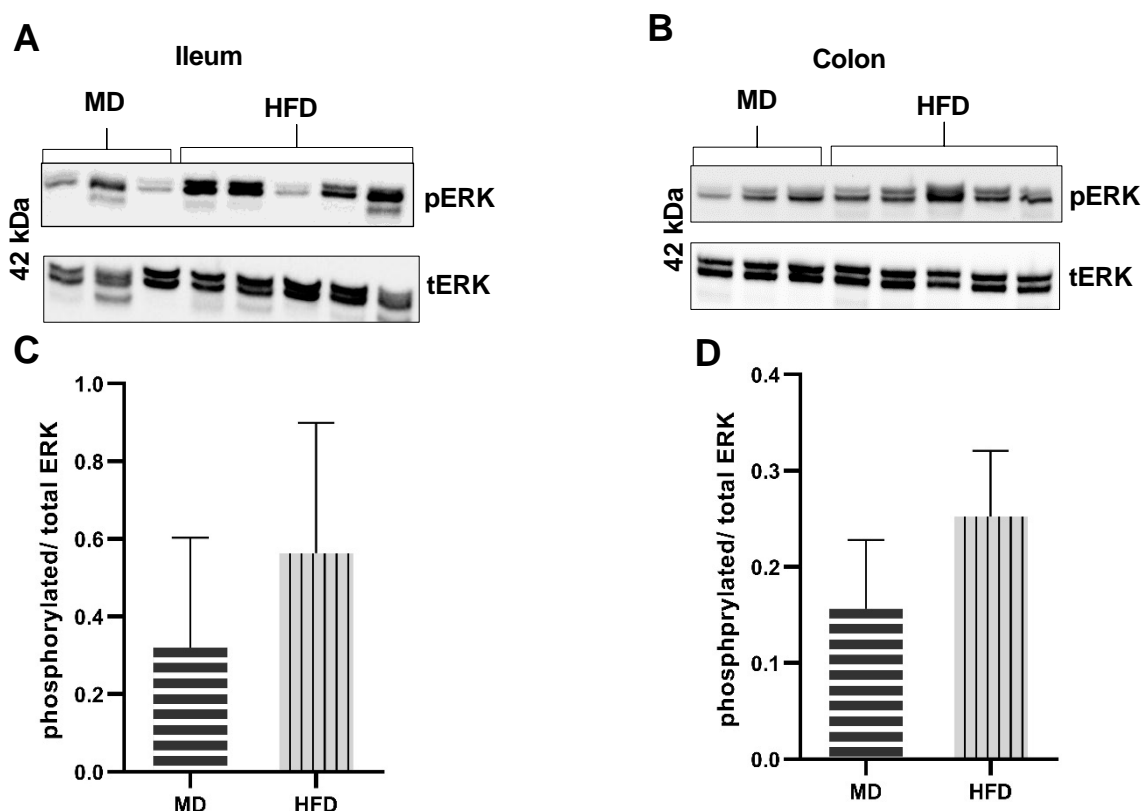
Figure 4.5: The effect of an HFD on the phosphorylation of intestinal ERK1/2 in vervet monkeys (*Chlorocebus aethiops*). Chemiluminescence images depicting the presence of pERK and tERK **(A, B)**. Phosphorylation of ERK1/2 is represented as phosphorylated/ total ERK. There were no differences in phosphorylation of ERK1/2 in the ileum and colon between MD-fed and HFD-fed vervet monkeys **(C, D)**. Abbreviations: maize-based diet (MD), high-fat diet (HFD), phosphorylated ERK (pERK) and total ERK (tERK).

The expression of a MAPK signalling pathway molecule, p38, was detected by western blot analysis and quantified using Image Lab software. Chemiluminescence images depicting bands indicative of the presence of p38 **(Figure 4.6A, B)**. There were no differences in the expression of total-p38 in the ileum (p=0.227) of HFD-fed vervet monkeys when compared to the MD-fed vervet monkeys **(Figure 4.6C)**. Also, there were no notable differences in the expression of total-p38 in the colon (p=0.673) between HFD-fed and MD-fed vervet monkeys **(Figure 4.6D)**.
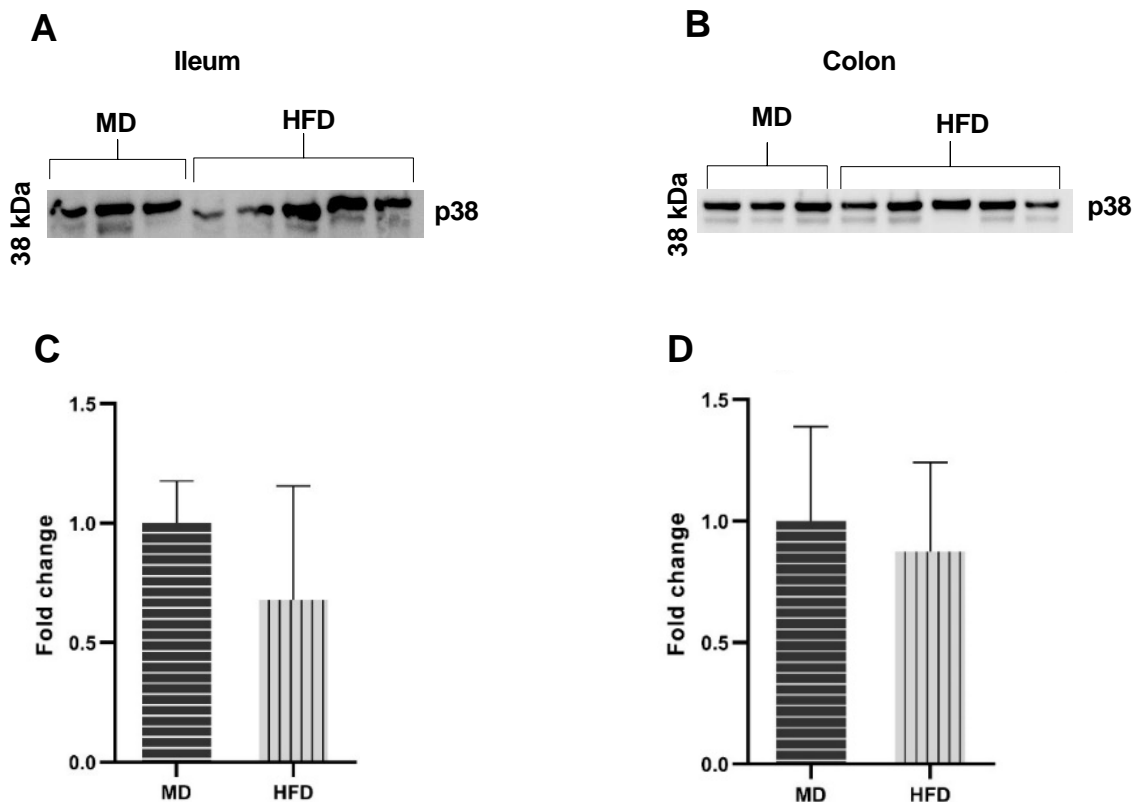
Figure 4.6: The effect of an HFD on p38 expression in the ileum and colon of vervet monkeys (*Chlorocebus aethiops*). Chemiluminescence images depicting the presence of p38 in the ileum and colon **(A, B)**. Protein expression is represented as fold change. There were no significant differences in total-p38 expression in the ileum and colon of the MD-fed vervet monkeys when compared to the HFD-fed vervet monkeys **(C, D)**. Abbreviations: maize-based diet (MD) and high-fat diet (HFD).

4.6. The effect of a high-fat diet on serum levels of biomarkers of leaky gut: LBP, and CD14

The effect of an HFD on serum levels (ng/mL) of biomarkers of metabolic endotoxemia (leaky gut), LBP and CD14 were determined using ELISA kits. There were no significant differences in serum levels of LBP (p=0.405) and CD14 (p=0.856) between the HFD-fed and MD-fed vervet monkeys **(Figure 4.7A, B)**.
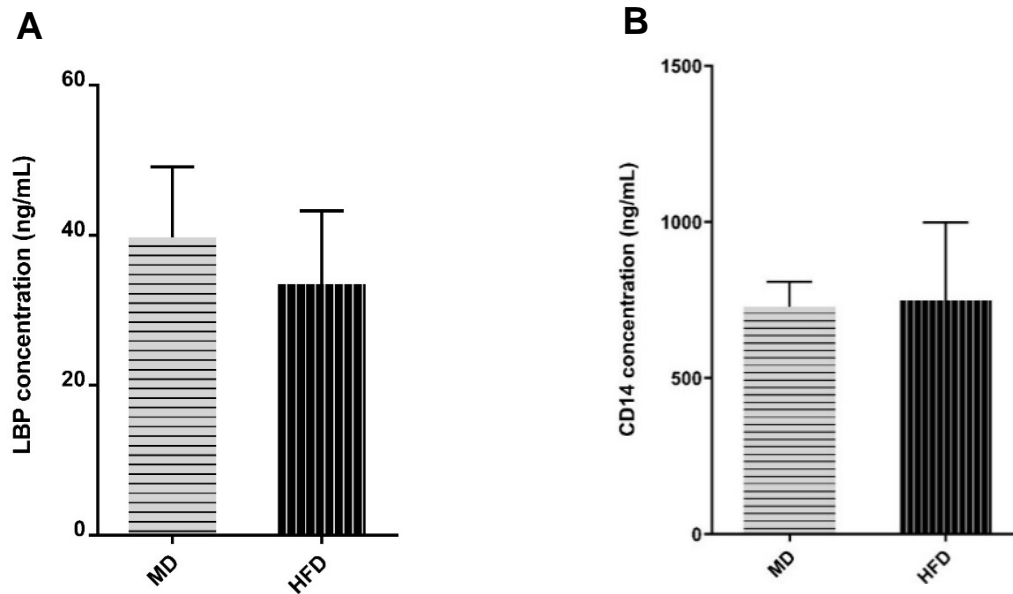
Figure 4.7: The effect of an HFD on serum levels of LBP and CD14 in vervet monkeys (*Chlorocebus aethiops*). There were no significant differences in serum levels of both LBP **(A)** and CD14 **(B)** between MD-fed and HFD-fed vervet monkeys. Abbreviations: maize-based diet (MD), high-fat diet (HFD), Lipopolysaccharide-binding protein (LBP) and cluster of differentiation 14 (CD14).

CHAPTER FIVE

5. Discussion

The rise in the consumption of Westernised HFDs has been reported to lead to intestinal barrier dysfunction, a significant cause of subclinical systemic and tissue inflammation which contributes to the development of metabolic disorders (Cani *et al.*, 2008; Christ *et al.*, 2019; Genser *et al.*, 2018;). Thus, there are continuous attempts to gain insight into the role of the intestinal barrier in the development of metabolic disorders following exposure to WDs (Malesza *et al.*, 2021). Understanding the role of the intestinal barrier in the development of metabolic disorders may help in the development of potential therapeutic and/ or preventive targets in intestinal barrier defects and downstream metabolic impairments. As such, this study investigated the long-term effects of an HFD on intestinal tissues and serum of aged (22.7 ± 2.3 years) vervet monkeys.

Non-human primates have been posited as a valuable model in investigating the pathophysiology of T2D due to the similarities in metabolic disorders such as insulin resistance, obesity and dyslipidaemia as observed in humans (Pound *et al.*, 2014). Impaired fasting glucose (characterised by FBG levels between 5.6-6.9 mmol/L) and HbA1c levels > 5.7% are strong predictors of diabetes risk in humans (Cavero-Redondo *et al.*, 2019; Kurotani *et al.*, 2017). Lu *et al.* (2015) reported no differences in HbA1c levels of rhesus monkeys fed an HFHSD when compared with ND-fed rhesus monkeys. They further reported that an HFHSD, induced significant differences in FBG when compared with ND-fed rhesus monkeys. Jin *et al.* (2019) also reported that the consumption of an HFD did not induce changes in FBG levels of cynomolgus monkeys. These authors, however, reported that an HFD led to impaired glucose tolerance following the oral glucose tolerance test. This study reports no significant differences in FBG levels and HbA1c levels between the HFD-fed and MD-fed monkeys **(Table 4.1)**, suggesting that an HFD did not affect glucose metabolism.

Dyslipidaemia, which involves an imbalance of HDL-C, LDL-C and TC in the blood, is considered one of the contributors to the development of T2D (Krauss, 2004). The consumption of WDs has been correlated with dyslipidaemia (Esmaillzadeh *et al.*, 2007). In this study, an HFD dysregulated lipid metabolism evidenced by a marginal increase in TC levels and significant increases in both LDL-C and HDL-C levels of

HFD-fed monkeys when compared to MD-fed monkeys **(Table 4.1)**. However, no differences were observed in TG levels between the HFD-fed and MD-fed monkeys **(Table 4.1)**. In line with this, a group of cynomolgus monkeys fed an HFD for 18 months was reported to have no differences in TG levels when compared to cynomolgus monkeys fed an ND (Jin *et al.*, 2019). Although Orlando *et al.* (2019) also reported that vervet monkeys fed an HFD and MD for 5 years had no differences in TG levels. The authors further reported that HFD-fed vervet monkeys developed dyslipidaemia evidenced by significantly elevated HDL-C, LDL-C and TC levels when compared to MD-fed vervet monkeys. The elevated LDL-C levels in this study may contribute to increased risk of T2D. Conversely, elevated HDL-C, while considered beneficial, may have nuanced effects on T2D outcomes such as improved insulin sensitivity based on factors such as HDL particle subtypes (Xepapadaki *et al.*, 2021). In particular, smaller TG-HDL rich particles have been associated with high plasma glucose levels (Liu *et al.*, 2017) whereas large HDL particles have been correlated with good glycaemic control (Tabara *et al.*, 2017). Further investigation is needed to comprehend the interplay between HFD, lipid profiles and T2D.

Quantitating intestinal morphology features such as villus length and crypt depth may provide insight into the intestinal function(s) (Xie *et al.*, 2020). Animal studies reporting on the effects of an HFD on intestinal morphology are contradictory, mice fed an HFD had decreased villus length in the jejunum and crypt depth in the colon when compared to mice fed an ND (Xie *et al.*, 2020). A study by Baldassano *et al.* (2013) revealed that HFD-fed mice had increased crypt-villus length in the duodenum and jejunum when compared to ND-fed mice, in addition, the HFD-fed mice became obese. Mice with HFD-induced obesity were reported to have increased villus length in the duodenum and jejunum (Baldassano *et al.*, 2013; Mah *et al.*, 2014; Mao *et al.*, 2013). Administration of an HFD in mice was reported to not affect the depth of intestinal crypts in the colon when compared to ND-fed mice (Navarrete *et al.*, 2015). Enriquez *et al.* (2022) reported no differences in villus height between HFD-fed and ND-fed mice in the duodenum and jejunum. In this study, no differences in the villus length (ileum) and crypt depth (colon) of both MD-fed and HFD-fed monkeys were observed **(Figure 4.1B, C)**. Factors such as dietary fat content and type of fat including animal model used (Spencer *et al.*, 1986; Malesza *et al.*, 2021) could have played a role in similarities of the intestinal morphology of both HFD-fed and MD-fed monkeys. In

future, increasing the sample size and using more dietary fat content than the one used in this study (40%) should be considered to better understand the effects of HFDs on intestinal morphology. Also, assessment of intestinal morphology in the duodenum and jejunum could have provided more insight into the effects of an HFD since these are sites exposed to a more dietary load, however they were excluded from analysis since they were autolysed **(described in 3.4.1)** . In addition, fat digestion and absorption occur in these regions (Hall and Hall, 2021). Nonetheless, the data in this study suggests that an HFD did not alter the morphology of the ileum and colon in vervet monkeys.

Plasma cells (IgA^+ cells) found in intestinal mucosal sites release sIgA into the intestinal lumen to defend against harmful antigens, bacteria, and pathogens (Brandtzaeg and Johansen, 2005). Furthermore, changes in gut mucosal immune cell populations have been linked with the development of metabolic diseases (Winer *et al.*, 2017). In this study, it was demonstrated that the population of IgA^+ cells in the duodenum of vervet monkeys fed an HFD was increased in comparison with MD-fed vervet monkeys **(Figure 4.3A)**. There were no differences in the population of IgA^+ cells in the jejunum, ileum and colon of HFD-fed and MD-fed vervet monkeys **(Figure 4.3B, C, D)**. Contrary to the findings in this study, Sakamoto *et al.* (2021) reported that mice fed an HFD had a low population of IgA^+ cells in the jejunum of mice when compared to mice fed an ND. Another study reported that the number of IgA^+ cells assessed by flow cytometry was reduced in the colon of HFD-fed mice when compared with ND-fed mice (Luck *et al.*, 2019). These authors also reported decreases in the number of IgA^+ cells assessed by IHC in the colon of HFD-fed mice when compared with ND-fed mice. In addition, insignificant differences in the population of IgA^+ cells in the distal small intestine (jejunum and ileum) of HFD-fed and ND-fed mice assessed using both flow cytometry and IHC were reported. Parker (2022) demonstrated that mice fed a high-sugar diet, had a significant increase in IgA^+ cells in the jejunum when compared to mice fed an ND. Thus, it is evident that the effect of WDs on IgA^+ cells varies. While speculative, an increase in the population of IgA^+ cells may indicate a compensatory defense mechanism to underlying mucosal damage which may have implications for the development of metabolic disease. Noteworthy, IgA is important in defence against harmful antigens, bacteria and pathogens, the increased IgA^+ cells in the duodenum in this study may suggest a

heightened immune response in the mucosal lining as a result of the HFD. The IgA$^+$ cells could be reacting to specific dietary components or gut microbial metabolites in response to the HFD. Variations in the distribution of immune cell populations along the intestine (Mowat and Agace, 2014), including different immune response signals due to varying luminal contents along the intestine and differences in the animal models used may further explain the findings in this study. Thus, further investigation is warranted to elucidate the precise mechanisms linking HFDs to intestinal barrier and mucosal immunity and their role in metabolic diseases.

The TJ protein complex between IECs is essential to prevent the paracellular permeability of unwanted substances that may cause either local or systemic inflammation (Cani *et al.*, 2012; Garcia-Hernandez *et al.*, 2017). Immunohistochemical analysis in the duodenum and jejunum of HFD-fed mice revealed that the expression of claudin-1, -2, and -3 and ZO-1 was decreased when compared to ND-fed mice (Nascimento *et al.*, 2021). This was associated with increased intestinal permeability evaluated by the fluorescein isothiocyanate-dextran assay. The expression of occludin, a TJ protein that plays a role in maintaining epithelial integrity (Saito *et al.*, 2021), was reported to be significantly decreased in the jejunum and ileum of HFD-fed mice when compared to MD-fed mice, and this was associated with increased intestinal permeability in the HFD group (Nakanishi *et al.*, 2021). This study reports no changes in occludin expression in the ileum and colon of HFD-fed and MD-fed vervet monkeys **(Figure 4.4B, C)**. Although the study by Nascimento *et al.* (2021) reported similar findings; no significant differences in the expression of occludin in the duodenum and jejunum of both HFD-fed and ND-fed mice. The authors, however, assessed the expression of other TJ proteins (previously mentioned), which were associated with increased intestinal permeability. Increased intestinal permeability results from impaired epithelial barrier integrity evidenced by dysregulation of TJ proteins (Turner, 2009). Assessing the expression of other TJ proteins could have provided possible evidence of impaired epithelial integrity, however, the undetectable antibodies specific for TJ proteins during western blot analysis **(Table 6.5)** prevented this.

The intestinal mucosal immune system interacts with luminal contents such as dietary antigens to maintain homeostasis and prevent unwanted pro-inflammatory immune responses which may consequently lead to metabolic endotoxemia (Cani *et al.*, 2007).

MAPKs play a role in the synthesis of pro-inflammatory mediators. MAPKs such as ERK1/2 can be activated by LPS and cytokines of the TNF family (Kyriakis and Avruch, 2012). Another MAPK, p38, has been suggested to be involved in mediating apoptosis following HFD-induced heart and liver tissue damage in mice (Li *et al.*, 2005). HFD-induced obese mice were reported to have increased expression of ERK1/2 and p38 in the small intestine when compared to non-obese mice fed an ND. These findings were associated with intestinal inflammation, and impaired glucose and lipid metabolism (Liu *et al.*, 2022). In line with this, Cremonini *et al.* (2019) reported that HFD-fed mice had increased expression of ERK1/2 in the ileum when compared with ND-fed mice. They attributed these findings to impaired epithelial barrier integrity characterised by decreased expression of ileal TJ proteins in HFD-fed mice. This study reports no significant changes in the expression of ERK1/2 in the ileum and colon between HFD-fed and MD-fed vervet monkeys **(Figure 4.5C, D)**. The same trend was observed in the expression of p38 in the ileum and colon of HFD-fed and MD-fed vervet monkeys **(Figure 4.6C, D)**. These findings may be associated with the reported insignificant changes in intestinal morphology **(Figure 4.1)**, and occludin expression **(Figure 4.4B, C)** between HFD-fed and MD-fed vervet monkeys used in this study, since intestinal inflammation is initiated by increased intestinal permeability (Rohr *et al.*, 2019). Furthermore, MAPKs have been reported to have pleiotropic effects at a molecular and tissue level such as apoptosis and proliferation (Arthur and Ley, 2013; Kyriakis and Avruch, 2012).

Metabolic endotoxemia is a condition characterised by a chronic pro-inflammatory state because of increased intestinal permeability of LPS into systemic circulation. Lipopolysaccharide is an endotoxin that stimulates TLR4 signalling, which leads to the recruitment of proteins such as LBP and CD14 (Pugin *et al.*, 1993). The formation of this complex triggers the release of pro-inflammatory cytokines implicated in T2D development (Cani *et al.*, 2007). Papoutsis *et al.* (2022) reported that an HFD did not induce significant differences in plasma levels of LBP in mice when compared to ND-fed mice. Conversely, mice fed an HFD were reported to have increased serum levels of LPB when compared to mice fed an ND (Dalby *et al.*, 2018; Stanisic *et al.*, 2021). Kavanagh *et al.* (2013) reported that cynomolgus and vervet monkeys fed a high-fructose diet had high plasma levels of LPS, CD14 and LBP. This study reports no significant differences in serum levels of LBP and CD14 between HFD-fed and MD-

fed vervet monkeys **(Figure 4.7A, B)**, suggesting that an HFD did not lead to metabolic endotoxemia. This may be corroborated by the invariable expression of epithelial barrier integrity (influences intestinal permeability) marker, occludin, in the ileum and colon of both HFD-fed and MD-fed vervet monkeys **(Figure 4.4B, C)**.

The results of this study revealed that an HFD dysregulated lipid metabolism in aged vervet monkeys, suggesting a possible predisposition to developing metabolic disease. In addition, an HFD increased the population of intestinal IgA^+ cells in the duodenum of vervet monkeys, suggesting dysregulated mucosal immune responses, however, further investigation is warranted to elucidate the mechanisms.

REFERENCES

Acheson, D.W.K. and Luccioli, S. (2004) 'Microbial-gut interactions in health and disease. Mucosal immune responses', *Best Practice & Research. Clinical Gastroenterology*, 18(2), pp. 387–404. Available at: https://doi.org/10.1016/j.bpg.2003.11.002.

Ahluwalia, B., Magnusson, M.K. and Öhman, L. (2017) 'Mucosal immune system of the gastrointestinal tract: maintaining balance between the good and the bad', *Scandinavian Journal of Gastroenterology*, 52(11), pp. 1185–1193. Available at: https://doi.org/10.1080/00365521.2017.1349173.

Antoni, L., Nuding, S., Weller, D., Gersemann, M., Ott, G., Wehkamp, J. and Stange, E.F. (2013) 'Human colonic mucus is a reservoir for antimicrobial peptides', *Journal of Crohn's & Colitis*, 7(12), pp. e652-664. Available at: https://doi.org/10.1016/j.crohns.2013.05.006.

Arthur, J.S.C. and Ley, S.C. (2013) 'Mitogen-activated protein kinases in innate immunity', *Nature Reviews Immunology*, 13(9), pp. 679–692. Available at: https://doi.org/10.1038/nri3495.

Artis, D. (2008) 'Epithelial-cell recognition of commensal bacteria and maintenance of immune homeostasis in the gut', *Nature Reviews. Immunology*, 8(6), pp. 411–420. Available at: https://doi.org/10.1038/nri2316.

Balda, M.S. and Matter, K. (2008) 'Tight junctions at a glance', *Journal of Cell Science*, 121(Pt 22), pp. 3677–3682. Available at: https://doi.org/10.1242/jcs.023887.

Balda, M.S., Whitney, J.A., Flores, C., González, S., Cereijido, M. and Matter, K. (1996) 'Functional dissociation of paracellular permeability and transepithelial electrical resistance and disruption of the apical-basolateral intramembrane diffusion barrier by expression of a mutant tight junction membrane protein', *The Journal of Cell Biology*, 134(4), pp. 1031–1049. Available at: https://doi.org/10.1083/jcb.134.4.1031.

Baldassano, S., Amato, A., Cappello, F., Rappa, F. and Mulè, F. (2013) 'Glucagon-like peptide-2 and mouse intestinal adaptation to a high-fat diet', *Journal of Endocrinology*, 217(1), pp. 11–20. Available at: https://doi.org/10.1530/JOE-12-0500.

Bergstrom, K.S.B., Kissoon-Singh, V., Gibson, D.L., Ma, C., Montero, M., Sham, H.P., Ryz, N., Huang, T., Velcich, A., Finlay, B.B., Chadee, K. and Vallance, B.A. (2010) 'Muc2 Protects against Lethal Infectious Colitis by Disassociating Pathogenic and Commensal Bacteria from the Colonic Mucosa', *PLoS Pathogens*. Edited by C.R. Roy, 6(5), p. e1000902. Available at: https://doi.org/10.1371/journal.ppat.1000902.

Birchenough, G.M.H., Johansson, M.E., Gustafsson, J.K., Bergström, J.H. and Hansson, G.C. (2015) 'New developments in goblet cell mucus secretion and function', *Mucosal Immunology*, 8(4), pp. 712–719. Available at: https://doi.org/10.1038/mi.2015.32.

Bogunovic, M., Davé, S.H., Tilstra, J.S., Chang, D.T.W., Harpaz, N., Xiong, H., Mayer, L.F. and Plevy, S.E. (2007) 'Enteroendocrine cells express functional Toll-like receptors', *American Journal of Physiology-Gastrointestinal and Liver Physiology*, 292(6), pp. G1770–G1783. Available at: https://doi.org/10.1152/ajpgi.00249.2006.

Booth, C. and Potten, C.S. (2000) 'Gut instincts: thoughts on intestinal epithelial stem cells', *The Journal of Clinical Investigation*, 105(11), pp. 1493–1499. Available at: https://doi.org/10.1172/JCI10229.

Brandtzaeg, P. and Johansen, F.-E. (2005) 'Mucosal B cells: phenotypic characteristics, transcriptional regulation, and homing properties', *Immunological Reviews*, 206(1), pp. 32–63. Available at: https://doi.org/10.1111/j.0105-2896.2005.00283.x.

Bremer, A.A., Stanhope, K.L., Graham, J.L., Cummings, B.P., Wang, W., Saville, B.R. and Havel, P.J. (2011) 'Fructose-fed rhesus monkeys: a nonhuman primate model of insulin resistance, metabolic syndrome, and type 2 diabetes', *Clinical and Translational Science*, 4(4), pp. 243–252. Available at: https://doi.org/10.1111/j.1752-8062.2011.00298.x.

Cani, P.D., Amar, J., Iglesias, M.A., Poggi, M., Knauf, C., Bastelica, D., Neyrinck, A.M., Fava, F., Tuohy, K.M., Chabo, C., Waget, A., Delmée, E., Cousin, B., Sulpice, T., Chamontin, B., Ferrières, J., Tanti, J.-F., Gibson, G.R., Casteilla, L., Delzenne, N.M., Alessi, M.C. and Burcelin, R. (2007) 'Metabolic Endotoxemia Initiates Obesity and Insulin Resistance', *Diabetes*, 56(7), pp. 1761–1772. Available at: https://doi.org/10.2337/db06-1491.

Cani, P.D., Bibiloni, R., Knauf, C., Waget, A., Neyrinck, A.M., Delzenne, N.M. and Burcelin, R. (2008) 'Changes in gut microbiota control metabolic endotoxemia-induced inflammation in high-fat diet-induced obesity and diabetes in mice', *Diabetes*, 57(6), pp. 1470–1481. Available at: https://doi.org/10.2337/db07-1403.

Cani, P.D., Osto, M., Geurts, L. and Everard, A. (2012) 'Involvement of gut microbiota in the development of low-grade inflammation and type 2 diabetes associated with obesity', *Gut Microbes*, 3(4), pp. 279–288. Available at: https://doi.org/10.4161/gmic.19625.

Cario, E. and Podolsky, D.K. (2000) 'Differential Alteration in Intestinal Epithelial Cell Expression of Toll-Like Receptor 3 (TLR3) and TLR4 in Inflammatory Bowel Disease', *Infection and Immunity*. Edited by J.D. Clements, 68(12), pp. 7010–7017. Available at: https://doi.org/10.1128/IAI.68.12.7010-7017.2000.

Cavero-Redondo, I., Martínez-Vizcaíno, V., Álvarez-Bueno, C., Agudo-Conde, C., Lugones-Sánchez, C. and García-Ortiz, L. (2019) 'Metabolic Syndrome Including Glycated Hemoglobin A1c in Adults: Is It Time to Change?', *Journal of Clinical Medicine*, 8(12), p. 2090. Available at: https://doi.org/10.3390/jcm8122090.

Chatterjee, S., Khunti, K. and Davies, M.J. (2017) 'Type 2 diabetes', *The Lancet*, 389(10085), pp. 2239–2251. Available at: https://doi.org/10.1016/S0140-6736(17)30058-2.

Chen, Y., Merzdorf, C., Paul, D.L. and Goodenough, D.A. (1997) 'COOH terminus of occludin is required for tight junction barrier function in early Xenopus embryos', *The Journal of Cell Biology*, 138(4), pp. 891–899. Available at: https://doi.org/10.1083/jcb.138.4.891.

Cheroutre, H., Lambolez, F. and Mucida, D. (2011) 'The light and dark sides of intestinal intraepithelial lymphocytes', *Nature Reviews Immunology*, 11(7), pp. 445–456. Available at: https://doi.org/10.1038/nri3007.

Choi, Y.J., Im, E., Chung, H.K., Pothoulakis, C. and Rhee, S.H. (2010) 'TRIF mediates Toll-like receptor 5-induced signaling in intestinal epithelial cells', *The Journal of Biological Chemistry*, 285(48), pp. 37570–37578. Available at: https://doi.org/10.1074/jbc.M110.158394.

Christ, A., Lauterbach, M. and Latz, E. (2019) 'Western Diet and the Immune System: An Inflammatory Connection', *Immunity*, 51(5), pp. 794–811. Available at: https://doi.org/10.1016/j.immuni.2019.09.020.

Conley, M.E. (1987) 'Intravascular and Mucosal Immunoglobulin A: Two Separate but Related Systems of Immune Defense?', *Annals of Internal Medicine*, 106(6), p. 892. Available at: https://doi.org/10.7326/0003-4819-106-6-892.

Cremonini, E., Daveri, E., Mastaloudis, A., Adamo, A.M., Mills, D., Kalanetra, K., Hester, S.N., Wood, S.M., Fraga, C.G. and Oteiza, P.I. (2019) 'Anthocyanins protect the gastrointestinal tract from high fat diet-induced alterations in redox signaling, barrier integrity and dysbiosis', *Redox Biology*, 26, p. 101269. Available at: https://doi.org/10.1016/j.redox.2019.101269.

Dalby, M.J., Aviello, G., Ross, A.W., Walker, A.W., Barrett, P. and Morgan, P.J. (2018) 'Diet induced obesity is independent of metabolic endotoxemia and TLR4 signalling, but markedly increases hypothalamic expression of the acute phase protein, SerpinA3N', *Scientific Reports*, 8(1), p. 15648. Available at: https://doi.org/10.1038/s41598-018-33928-4.

Deplancke, B. and Gaskins, H.R. (2001) 'Microbial modulation of innate defense: goblet cells and the intestinal mucus layer', *The American Journal of Clinical Nutrition*, 73(6), pp. 1131S-1141S. Available at: https://doi.org/10.1093/ajcn/73.6.1131S.

Dunst, S. and Tomancak, P. (2019) 'Imaging Flies by Fluorescence Microscopy: Principles, Technologies, and Applications', *Genetics*, 211(1), pp. 15–34. Available at: https://doi.org/10.1534/genetics.118.300227.

Ehmann, D., Wendler, J., Koeninger, L., Larsen, I.S., Klag, T., Berger, J., Marette, A., Schaller, M., Stange, E.F., Malek, N.P., Jensen, B. a. H. and Wehkamp, J. (2019) 'Paneth cell α-defensins HD-5 and HD-6 display differential degradation into active antimicrobial fragments', *Proceedings of the National Academy of Sciences of the United States of America*, 116(9), pp. 3746–3751. Available at: https://doi.org/10.1073/pnas.1817376116.

Engle, M.J., Mahmood, A. and Alpers, D.H. (1995) 'Two Rat Intestinal Alkaline Phosphatase Isoforms with Different Carboxyl-terminal Peptides Are Both Membrane-

bound by a Glycan Phosphatidylinositol Linkage', *Journal of Biological Chemistry*, 270(20), pp. 11935–11940. Available at: https://doi.org/10.1074/jbc.270.20.11935.

Enriquez, J.R., McCauley, H.A., Zhang, K.X., Sanchez, J.G., Kalin, G.T., Lang, R.A. and Wells, J.M. (2022) 'A dietary change to a high-fat diet initiates a rapid adaptation of the intestine', *Cell Reports*, 41(7), p. 111641. Available at: https://doi.org/10.1016/j.celrep.2022.111641.

Eri, R. and Chieppa, M. (2013) 'Messages from the Inside. The Dynamic Environment that Favors Intestinal Homeostasis', *Frontiers in Immunology*, 4, p. 323. Available at: https://doi.org/10.3389/fimmu.2013.00323.

Ermund, A., Schütte, A., Johansson, M.E.V., Gustafsson, J.K. and Hansson, G.C. (2013) 'Studies of mucus in mouse stomach, small intestine, and colon. I. Gastrointestinal mucus layers have different properties depending on location as well as over the Peyer's patches', *American Journal of Physiology. Gastrointestinal and Liver Physiology*, 305(5), pp. G341-347. Available at: https://doi.org/10.1152/ajpgi.00046.2013.

Eroschenko, V.P. and Fiore, M.S.H. di (2013) *DiFiore's Atlas of Histology with Functional Correlations*. Lippincott Williams & Wilkins.

Esmaillzadeh, A., Kimiagar, M., Mehrabi, Y., Azadbakht, L., Hu, F.B. and Willett, W.C. (2007) 'Dietary patterns, insulin resistance, and prevalence of the metabolic syndrome in women', *The American Journal of Clinical Nutrition*, 85(3), pp. 910–918. Available at: https://doi.org/10.1093/ajcn/85.3.910.

Fagarasan, S. and Honjo, T. (2003) 'Intestinal IgA synthesis: regulation of front-line body defences', *Nature Reviews. Immunology*, 3(1), pp. 63–72. Available at: https://doi.org/10.1038/nri982.

Fang, J., Sun, X., Xue, B., Fang, N. and Zhou, M. (2017) 'Dahuang Zexie Decoction Protects against High-Fat Diet-Induced NAFLD by Modulating Gut Microbiota-Mediated Toll-Like Receptor 4 Signaling Activation and Loss of Intestinal Barrier', *Evidence-Based Complementary and Alternative Medicine*, 2017, pp. 1–13. Available at: https://doi.org/10.1155/2017/2945803.

Fenton, T.M., Jørgensen, P.B., Niss, K., Rubin, S.J.S., Mörbe, U.M., Riis, L.B., Da Silva, C., Plumb, A., Vandamme, J., Jakobsen, H.L., Brunak, S., Habtezion, A., Nielsen, O.H., Johansson-Lindbom, B. and Agace, W.W. (2020) 'Immune Profiling of Human Gut-Associated Lymphoid Tissue Identifies a Role for Isolated Lymphoid Follicles in Priming of Region-Specific Immunity', *Immunity*, 52(3), pp. 557-570.e6. Available at: https://doi.org/10.1016/j.immuni.2020.02.001.

Fernandez, M.I., Pedron, T., Tournebize, R., Olivo-Marin, J.-C., Sansonetti, P.J. and Phalipon, A. (2003) 'Anti-Inflammatory Role for Intracellular Dimeric Immunoglobulin A by Neutralization of Lipopolysaccharide in Epithelial Cells', *Immunity*, 18(6), pp. 739–749. Available at: https://doi.org/10.1016/S1074-7613(03)00122-5.

Fincham, J.E., Faber, M., Weight, M.J., Labadarios, D., Taljaard, J.J., Steytler, J.G., Jacobs, P. and Kritchevsky, D. (1987) 'Diets realistic for westernized people significantly effect lipoproteins, calcium, zinc, vitamins C, E, B6 and haematology in vervet monkeys', *Atherosclerosis*, 66(3), pp. 191–203. Available at: https://doi.org/10.1016/0021-9150(87)90063-3.

Gao, J.-M., Rao, J.-H., Wei, Z.-Y., Xia, S.-Y., Huang, L., Tang, M.-T., Hide, G., Zheng, T.-T., Li, J.-H., Zhao, G.-A., Sun, Y.-X. and Chen, J.-H. (2022) 'Transplantation of Gut Microbiota From High-Fat-Diet-Tolerant Cynomolgus Monkeys Alleviates Hyperlipidemia and Hepatic Steatosis in Rats', *Frontiers in Microbiology*, 13, p. 876043. Available at: https://doi.org/10.3389/fmicb.2022.876043.

Garcia, M.A., Nelson, W.J. and Chavez, N. (2018) 'Cell–Cell Junctions Organize Structural and Signaling Networks', *Cold Spring Harbor Perspectives in Biology*, 10(4), p. a029181. Available at: https://doi.org/10.1101/cshperspect.a029181.

Garcia-Hernandez, V., Quiros, M. and Nusrat, A. (2017) 'Intestinal epithelial claudins: expression and regulation in homeostasis and inflammation', *Annals of the New York Academy of Sciences*, 1397(1), pp. 66–79. Available at: https://doi.org/10.1111/nyas.13360.

Genser, L., Aguanno, D., Soula, H.A., Dong, L., Trystram, L., Assmann, K., Salem, J.-E., Vaillant, J.-C., Oppert, J.-M., Laugerette, F., Michalski, M.-C., Wind, P., Rousset, M., Brot-Laroche, E., Leturque, A., Clément, K., Thenet, S. and Poitou, C. (2018) 'Increased jejunal permeability in human obesity is revealed by a lipid challenge and

is linked to inflammation and type 2 diabetes', *The Journal of Pathology*, 246(2), pp. 217–230. Available at: https://doi.org/10.1002/path.5134.

Ghosh, S.S. (2020) 'Intestinal barrier function and metabolic/liver diseases', *Liver Research*, p. 7.

Gieryńska, M., Szulc-Dąbrowska, L., Struzik, J., Mielcarska, M.B. and Gregorczyk-Zboroch, K.P. (2022) 'Integrity of the Intestinal Barrier: The Involvement of Epithelial Cells and Microbiota—A Mutual Relationship', *Animals*, 12(2), p. 145. Available at: https://doi.org/10.3390/ani12020145.

Gommerman, J.L., Rojas, O.L. and Fritz, J.H. (2014) 'Re-thinking the functions of IgA(+) plasma cells', *Gut Microbes*, 5(5), pp. 652–662. Available at: https://doi.org/10.4161/19490976.2014.969977.

Gong, L., Zeng, W., Yang, Z., Chen, Z., Cheng, A., Shen, Y., Zeng, L., Luo, Q. and Yang, Y. (2013) 'Comparison of the clinical manifestations of type 2 diabetes mellitus between rhesus monkey (Macaca mulatta lasiotis) and human being', *Pancreas*, 42(3), pp. 537–542. Available at: https://doi.org/10.1097/MPA.0b013e3182732501.

Hall, J.E. and Hall, M.E. (2021) *Digestion and Absorption in the Gastrointestinal Tract-Guyton and Hall Textbook of Medical Physiology*. 14th edn. Elsevier. Available at: https://www.clinicalkey.com/#!/content/book/3-s2.0-B9780323597128000667?scrollTo=%23hl0000316 (Accessed: 24 February 2023).

Hamada, H., Hiroi, T., Nishiyama, Y., Takahashi, H., Masunaga, Y., Hachimura, S., Kaminogawa, S., Takahashi-Iwanaga, H., Iwanaga, T., Kiyono, H., Yamamoto, H. and Ishikawa, H. (2002) 'Identification of Multiple Isolated Lymphoid Follicles on the Antimesenteric Wall of the Mouse Small Intestine', *The Journal of Immunology*, 168(1), pp. 57–64. Available at: https://doi.org/10.4049/jimmunol.168.1.57.

Hansson, G.C. (2020) 'Mucins and the Microbiome', *Annual Review of Biochemistry*, 89(1), pp. 769–793. Available at: https://doi.org/10.1146/annurev-biochem-011520-105053.

Hao, W., Hao, C., Wu, C., Xu, Y. and Jin, C. (2022) 'Aluminum induced intestinal dysfunction via mechanical, immune, chemical and biological barriers', *Chemosphere*, 288, p. 132556. Available at: https://doi.org/10.1016/j.chemosphere.2021.132556.

Hasnain, S.Z., Wang, H., Ghia, J., Haq, N., Deng, Y., Velcich, A., Grencis, R.K., Thornton, D.J. and Khan, W.I. (2010) 'Mucin Gene Deficiency in Mice Impairs Host Resistance to an Enteric Parasitic Infection', *Gastroenterology*, 138(5), pp. 1763-1771.e5. Available at: https://doi.org/10.1053/j.gastro.2010.01.045.

Havel, P.J., Kievit, P., Comuzzie, A.G. and Bremer, A.A. (2017) 'Use and Importance of Nonhuman Primates in Metabolic Disease Research: Current State of the Field', *ILAR Journal*, 58(2), pp. 251–268. Available at: https://doi.org/10.1093/ilar/ilx031.

Higgins, P.B., Bastarrachea, R.A., Lopez-Alvarenga, J.C., Garcia-Forey, M., Proffitt, J.M., Voruganti, V.S., Tejero, M.E., Mattern, V., Haack, K., Shade, R.E., Cole, S.A. and Comuzzie, A.G. (2010) 'Eight week exposure to a high sugar high fat diet results in adiposity gain and alterations in metabolic biomarkers in baboons (Papio hamadryas sp.)', *Cardiovascular Diabetology*, 9, p. 71. Available at: https://doi.org/10.1186/1475-2840-9-71.

Holmes, J.L., Van Itallie, C.M., Rasmussen, J.E. and Anderson, J.M. (2006) 'Claudin profiling in the mouse during postnatal intestinal development and along the gastrointestinal tract reveals complex expression patterns', *Gene expression patterns: GEP*, 6(6), pp. 581–588. Available at: https://doi.org/10.1016/j.modgep.2005.12.001.

Imamura, F., Micha, R., Khatibzadeh, S., Fahimi, S., Shi, P., Powles, J., Mozaffarian, D., and Global Burden of Diseases Nutrition and Chronic Diseases Expert Group (NutriCoDE) (2015) 'Dietary quality among men and women in 187 countries in 1990 and 2010: a systematic assessment', *The Lancet. Global Health*, 3(3), pp. e132-142. Available at: https://doi.org/10.1016/S2214-109X(14)70381-X.

Jin, L.-S., Rao, J.-H., Zhang, L.-B., Ji, F., Zhang, Y.-C., Hao, X.-F., Peng, B.-L., Liu, X.-M. and Sun, Y.-X. (2019) 'Comparison of gene expression in cynomolgus monkeys with preclinical type II diabetes induced by different high energy diets', *Animal Models and Experimental Medicine*, 2(1), pp. 44–50. Available at: https://doi.org/10.1002/ame2.12058.

Katikireddy, K.R. and O'Sullivan, F. (2011) 'Immunohistochemical and Immunofluorescence Procedures for Protein Analysis', in L. O'Driscoll (ed.) *Gene Expression Profiling*. Totowa, NJ: Humana Press (Methods in Molecular Biology), pp. 155–167. Available at: https://doi.org/10.1007/978-1-61779-289-2_11.

Kavanagh, K., Fairbanks, L.A., Bailey, J.N., Jorgensen, M.J., Wilson, M., Zhang, L., Rudel, L.L. and Wagner, J.D. (2007) 'Characterization and heritability of obesity and associated risk factors in vervet monkeys', *Obesity (Silver Spring, Md.)*, 15(7), pp. 1666–1674. Available at: https://doi.org/10.1038/oby.2007.199.

Kavanagh, K., Wylie, A.T., Tucker, K.L., Hamp, T.J., Gharaibeh, R.Z., Fodor, A.A. and Cullen, J.M.C. (2013) 'Dietary fructose induces endotoxemia and hepatic injury in calorically controlled primates', *The American Journal of Clinical Nutrition*, 98(2), pp. 349–357. Available at: https://doi.org/10.3945/ajcn.112.057331.

Kawasaki, T. and Kawai, T. (2014) 'Toll-like receptor signaling pathways', *Frontiers in Immunology*, 5, p. 461. Available at: https://doi.org/10.3389/fimmu.2014.00461.

Keshav, S. (2006) 'Paneth cells: leukocyte-like mediators of innate immunity in the intestine', *Journal of Leukocyte Biology*, 80(3), pp. 500–508. Available at: https://doi.org/10.1189/jlb.1005556.

Khoshbin, K. and Camilleri, M. (2020) 'Effects of dietary components on intestinal permeability in health and disease', *American Journal of Physiology. Gastrointestinal and Liver Physiology*, 319(5), pp. G589–G608. Available at: https://doi.org/10.1152/ajpgi.00245.2020.

Kim, K.-A., Gu, W., Lee, I.-A., Joh, E.-H. and Kim, D.-H. (2012) 'High fat diet-induced gut microbiota exacerbates inflammation and obesity in mice via the TLR4 signaling pathway', *PloS One*, 7(10), p. e47713. Available at: https://doi.org/10.1371/journal.pone.0047713.

Kim, Y.S. and Ho, S.B. (2010) 'Intestinal goblet cells and mucins in health and disease: recent insights and progress', *Current Gastroenterology Reports*, 12(5), pp. 319–330. Available at: https://doi.org/10.1007/s11894-010-0131-2.

König, J., Wells, J., Cani, P.D., García-Ródenas, C.L., MacDonald, T., Mercenier, A., Whyte, J., Troost, F. and Brummer, R.-J. (2016) 'Human Intestinal Barrier Function in Health and Disease', *Clinical and Translational Gastroenterology*, 7(10), p. e196. Available at: https://doi.org/10.1038/ctg.2016.54.

Krauss, R.M. (2004) 'Lipids and lipoproteins in patients with type 2 diabetes', *Diabetes Care*, 27(6), pp. 1496–1504. Available at: https://doi.org/10.2337/diacare.27.6.1496.

Kurotani, K., Miyamoto, T., Kochi, T., Eguchi, M., Imai, T., Nishihara, A., Tomita, K., Uehara, A., Yamamoto, M., Murakami, T., Shimizu, C., Shimizu, M., Nagahama, S., Nakagawa, T., Honda, T., Yamamoto, S., Okazaki, H., Sasaki, N., Hori, A., Nishiura, C., Kuwahara, K., Kuroda, R., Akter, S., Kashino, I., Nanri, A., Kabe, I., Mizoue, T., Kunugita, N., Dohi, S., and Japan Epidemiology Collaboration on Occupational Health Study Group (2017) 'Metabolic syndrome components and diabetes incidence according to the presence or absence of impaired fasting glucose: The Japan Epidemiology Collaboration on Occupational Health Study', *Journal of Epidemiology*, 27(9), pp. 408–412. Available at: https://doi.org/10.1016/j.je.2016.08.015.

Kyriakis, J.M. and Avruch, J. (2012) 'Mammalian MAPK Signal Transduction Pathways Activated by Stress and Inflammation: A 10-Year Update', *Physiological Reviews*, 92(2), pp. 689–737. Available at: https://doi.org/10.1152/physrev.00028.2011.

Leong, K.W. and Ding, J.L. (2014) 'The Unexplored Roles of Human Serum IgA', *DNA and Cell Biology*, 33(12), pp. 823–829. Available at: https://doi.org/10.1089/dna.2014.2639.

Li, S.-Y., Liu, Y., Sigmon, V.K., McCort, A. and Ren, J. (2005) 'High-fat diet enhances visceral advanced glycation end products, nuclear O-Glc-Nac modification, p38 mitogen-activated protein kinase activation and apoptosis', *Diabetes, Obesity & Metabolism*, 7(4), pp. 448–454. Available at: https://doi.org/10.1111/j.1463-1326.2004.00387.x.

Liévin-Le Moal, V. and Servin, A.L. (2006) 'The front line of enteric host defense against unwelcome intrusion of harmful microorganisms: mucins, antimicrobial peptides, and microbiota', *Clinical Microbiology Reviews*, 19(2), pp. 315–337. Available at: https://doi.org/10.1128/CMR.19.2.315-337.2006.

Liu, J., van Klinken, J.B., Semiz, S., van Dijk, K.W., Verhoeven, A., Hankemeier, T., Harms, A.C., Sijbrands, E., Sheehan, N.A., van Duijn, C.M. and Demirkan, A. (2017) 'A Mendelian Randomization Study of Metabolite Profiles, Fasting Glucose, and Type 2 Diabetes', *Diabetes*, 66(11), pp. 2915–2926. Available at: https://doi.org/10.2337/db17-0199.

Liu, X. and Zhu, H. (2022) 'Curcumin Improved Intestinal Epithelial Barrier Integrity by Up-Regulating ZO-1/Occludin/Claudin-1 in Septic Rats', *Evidence-Based*

Complementary and Alternative Medicine: eCAM, 2022, p. 2884522. Available at: https://doi.org/10.1155/2022/2884522.

Liu, Y., Han, X., Cai, M., Jin, S., Yan, Z., Lu, H. and Chen, Q. (2022) 'Jianpi Qinghua Fomula alleviates insulin resistance via restraining of MAPK pathway to suppress inflammation of the small intestine in DIO mice', *BMC complementary medicine and therapies*, 22(1), p. 129. Available at: https://doi.org/10.1186/s12906-022-03595-0.

Lu, S., Qi, S., Zhao, Y., Li, Y., Yang, F., Yu, W., Jin, M., Chen, L.-X., Wang, J., He, Z. and Li, H. (2015) 'Type 2 diabetes mellitus non-genetic Rhesus monkey model induced by high fat and high sucrose diet', *Experimental and Clinical Endocrinology & Diabetes: Official Journal, German Society of Endocrinology [and] German Diabetes Association*, 123(1), pp. 19–26. Available at: https://doi.org/10.1055/s-0034-1385923.

Luck, H., Khan, S., Kim, J.H., Copeland, J.K., Revelo, X.S., Tsai, S., Chakraborty, M., Cheng, K., Tao Chan, Y., Nøhr, M.K., Clemente-Casares, X., Perry, M.-C., Ghazarian, M., Lei, H., Lin, Y.-H., Coburn, B., Okrainec, A., Jackson, T., Poutanen, S., Gaisano, H., Allard, J.P., Guttman, D.S., Conner, M.E., Winer, S. and Winer, D.A. (2019) 'Gut-associated IgA+ immune cells regulate obesity-related insulin resistance', *Nature Communications*, 10(1), p. 3650. Available at: https://doi.org/10.1038/s41467-019-11370-y.

Mah, A.T., Van Landeghem, L., Gavin, H.E., Magness, S.T. and Lund, P.K. (2014) 'Impact of Diet-Induced Obesity on Intestinal Stem Cells: Hyperproliferation but Impaired Intrinsic Function That Requires Insulin/IGF1', *Endocrinology*, 155(9), pp. 3302–3314. Available at: https://doi.org/10.1210/en.2014-1112.

Maldonado-Contreras, A.L. and McCormick, B.A. (2011) 'Intestinal epithelial cells and their role in innate mucosal immunity', *Cell and Tissue Research*, 343(1), pp. 5–12. Available at: https://doi.org/10.1007/s00441-010-1082-5.

Malesza, I.J., Malesza, M., Walkowiak, J., Mussin, N., Walkowiak, D., Aringazina, R., Bartkowiak-Wieczorek, J. and Mądry, E. (2021) 'High-Fat, Western-Style Diet, Systemic Inflammation, and Gut Microbiota: A Narrative Review', *Cells*, 10(11), p. 3164. Available at: https://doi.org/10.3390/cells10113164.

Mantis, N.J. and Forbes, S.J. (2010) 'Secretory IgA: arresting microbial pathogens at epithelial borders', *Immunological Investigations*, 39(4–5), pp. 383–406. Available at: https://doi.org/10.3109/08820131003622635.

Mantis, N.J., Rol, N. and Corthésy, B. (2011) 'Secretory IgA's complex roles in immunity and mucosal homeostasis in the gut', *Mucosal Immunology*, 4(6), pp. 603–611. Available at: https://doi.org/10.1038/mi.2011.41.

Mao, J., Hu, X., Xiao, Y., Yang, C., Ding, Y., Hou, N., Wang, J., Cheng, H. and Zhang, X. (2013) 'Overnutrition stimulates intestinal epithelium proliferation through β-catenin signaling in obese mice', *Diabetes*, 62(11), pp. 3736–3746. Available at: https://doi.org/10.2337/db13-0035.

Marshman, E., Booth, C. and Potten, C.S. (2002) 'The intestinal epithelial stem cell', *BioEssays: News and Reviews in Molecular, Cellular and Developmental Biology*, 24(1), pp. 91–98. Available at: https://doi.org/10.1002/bies.10028.

Mestecky, J., Russell, M.W., Jackson, S. and Brown, T.A. (1986) 'The human IgA system: a reassessment', *Clinical Immunology and Immunopathology*, 40(1), pp. 105–114. Available at: https://doi.org/10.1016/0090-1229(86)90073-5.

Miller, H. (2007) 'Intestinal M cells: The fallible sentinels?', *World Journal of Gastroenterology*, 13(10), p. 1477. Available at: https://doi.org/10.3748/wjg.v13.i10.1477.

Miron, N. and Cristea, V. (2012) 'Enterocytes: active cells in tolerance to food and microbial antigens in the gut', *Clinical and Experimental Immunology*, 167(3), pp. 405–412. Available at: https://doi.org/10.1111/j.1365-2249.2011.04523.x.

Mohammad, S. and Thiemermann, C. (2021) 'Role of Metabolic Endotoxemia in Systemic Inflammation and Potential Interventions', *Frontiers in Immunology*, 11, p. 594150. Available at: https://doi.org/10.3389/fimmu.2020.594150.

Mookherjee, N., Brown, K.L., Bowdish, D.M.E., Doria, S., Falsafi, R., Hokamp, K., Roche, F.M., Mu, R., Doho, G.H., Pistolic, J., Powers, J.-P., Bryan, J., Brinkman, F.S.L. and Hancock, R.E.W. (2006) 'Modulation of the TLR-Mediated Inflammatory Response by the Endogenous Human Host Defense Peptide LL-37', *The Journal of*

Immunology, 176(4), pp. 2455–2464. Available at: https://doi.org/10.4049/jimmunol.176.4.2455.

Mörbe, U.M., Jørgensen, P.B., Fenton, T.M., von Burg, N., Riis, L.B., Spencer, J. and Agace, W.W. (2021) 'Human gut-associated lymphoid tissues (GALT); diversity, structure, and function', *Mucosal Immunology*, 14(4), pp. 793–802. Available at: https://doi.org/10.1038/s41385-021-00389-4.

Mowat, A.M. and Agace, W.W. (2014) 'Regional specialization within the intestinal immune system', *Nature Reviews. Immunology*, 14(10), pp. 667–685. Available at: https://doi.org/10.1038/nri3738.

Mowat, A.Mcl. (2003) 'Anatomical basis of tolerance and immunity to intestinal antigens', *Nature Reviews Immunology*, 3(4), pp. 331–341. Available at: https://doi.org/10.1038/nri1057.

Mozaffarian, D. (2016) 'Dietary and Policy Priorities for Cardiovascular Disease, Diabetes, and Obesity: A Comprehensive Review', *Circulation*, 133(2), pp. 187–225. Available at: https://doi.org/10.1161/CIRCULATIONAHA.115.018585.

Muhomah, T.A., Nishino, N., Katsumata, E., Haoming, W. and Tsuruta, T. (2019) 'High-fat diet reduces the level of secretory immunoglobulin A coating of commensal gut microbiota', *Bioscience of Microbiota, Food and Health*, 38(2), pp. 55–64. Available at: https://doi.org/10.12938/bmfh.18-027.

Nagpal, R., Shively, C.A., Appt, S.A., Register, T.C., Michalson, K.T., Vitolins, M.Z. and Yadav, H. (2018) 'Gut Microbiome Composition in Non-human Primates Consuming a Western or Mediterranean Diet', *Frontiers in Nutrition*, 5, p. 28. Available at: https://doi.org/10.3389/fnut.2018.00028.

Nakanishi, T., Fukui, H., Wang, X., Nishiumi, S., Yokota, H., Makizaki, Y., Tanaka, Y., Ohno, H., Tomita, T., Oshima, T. and Miwa, H. (2021) 'Effect of a High-Fat Diet on the Small-Intestinal Environment and Mucosal Integrity in the Gut-Liver Axis', *Cells*, 10(11), p. 3168. Available at: https://doi.org/10.3390/cells10113168.

Nascimento, J.C., Matheus, V.A., Oliveira, R.B., Tada, S.F.S. and Collares-Buzato, C.B. (2021) 'High-Fat Diet Induces Disruption of the Tight Junction-Mediated Paracellular Barrier in the Proximal Small Intestine Before the Onset of Type 2

Diabetes and Endotoxemia', *Digestive Diseases and Sciences*, 66(10), pp. 3359–3374. Available at: https://doi.org/10.1007/s10620-020-06664-x.

Natali Almeida, F., Lucca Andrade, M., Marta Franzói de Moraes, S., Chimin, P., Natali de Almeida, K., Marina Peralta, R. and Marçal Natali, M.R. (2014) 'Obese adult phenotype: Adaptations of small intestine to cafeteria diet and aerobic physical training after weaning', *Science & Sports*, 29(1), pp. 20–26. Available at: https://doi.org/10.1016/j.scispo.2013.04.004.

Navarrete, J., Vásquez, B. and Del Sol, M. (2015) 'Morphoquantitative analysis of the Ileum of C57BL/6 mice (Mus musculus) fed with a high-fat diet', *International Journal of Clinical and Experimental Pathology*, 8(11), pp. 14649–14657.

Newman, T.M., Shively, C.A., Register, T.C., Appt, S.E., Yadav, H., Colwell, R.R., Fanelli, B., Dadlani, M., Graubics, K., Nguyen, U.T., Ramamoorthy, S., Uberseder, B., Clear, K.Y.J., Wilson, A.S., Reeves, K.D., Chappell, M.C., Tooze, J.A. and Cook, K.L. (2021) 'Diet, obesity, and the gut microbiome as determinants modulating metabolic outcomes in a non-human primate model', *Microbiome*, 9(1), p. 100. Available at: https://doi.org/10.1186/s40168-021-01069-y.

Nicholas, M.W. and Nelson, K. (2013) 'North, South, or East? Blotting Techniques', *Journal of Investigative Dermatology*, 133(7), pp. 1–3. Available at: https://doi.org/10.1038/jid.2013.216.

Niyonsaba, F., Iwabuchi, K., Someya, A., Hirata, M., Matsuda, H., Ogawa, H. and Nagaoka, I. (2002) 'A cathelicidin family of human antibacterial peptide LL-37 induces mast cell chemotaxis', *Immunology*, 106(1), pp. 20–26. Available at: https://doi.org/10.1046/j.1365-2567.2002.01398.x.

Okumura, R. and Takeda, K. (2017) 'Roles of intestinal epithelial cells in the maintenance of gut homeostasis', *Experimental & Molecular Medicine*, 49(5), p. e338. Available at: https://doi.org/10.1038/emm.2017.20.

Okyere, S.K., Wen, J., Cui, Y., Xie, L., Gao, P., Zhang, M., Wang, J., Wang, S., Ran, Y., Ren, Z. and Hu, Y. (2022) 'Bacillus toyonensis SAU-19 and SAU-20 Isolated From Ageratina adenophora Alleviates the Intestinal Structure and Integrity Damage

Associated With Gut Dysbiosis in Mice Fed High Fat Diet', *Frontiers in Microbiology*, 13, p. 820236. Available at: https://doi.org/10.3389/fmicb.2022.820236.

Orlando, P., Chellan, N., Louw, J., Tiano, L., Cirilli, I., Dludla, P., Joubert, E. and Muller, C.J.F. (2019) 'Aspalathin-Rich Green Rooibos Extract Lowers LDL-Cholesterol and Oxidative Status in High-Fat Diet-Induced Diabetic Vervet Monkeys', *Molecules*, 24(9), p. 1713. Available at: https://doi.org/10.3390/molecules24091713.

Otte, J.-M., Cario, E. and Podolsky, D.K. (2004) 'Mechanisms of cross hyporesponsiveness to toll-like receptor bacterial ligands in intestinal epithelial cells☆', *Gastroenterology*, 126(4), pp. 1054–1070. Available at: https://doi.org/10.1053/j.gastro.2004.01.007.

Pabst, O. (2012) 'New concepts in the generation and functions of IgA', *Nature Reviews. Immunology*, 12(12), pp. 821–832. Available at: https://doi.org/10.1038/nri3322.

Papoutsis, D., da Rocha, S.D.C., Herfindal, A.M., Bøhn, S.K. and Carlsen, H. (2022) 'A High-Fat Western Diet Attenuates Intestinal Changes in Mice with DSS-Induced Low-Grade Inflammation', *The Journal of Nutrition*, 152(3), pp. 758–769. Available at: https://doi.org/10.1093/jn/nxab401.

Parker, K. (2022) *The role of the intestinal immune system in the development and treatment of type 2 diabetes*. Stellenbosch University. Available at: http://hdl.handle.net/10019.1/126061.

Pelaseyed, T., Bergström, J.H., Gustafsson, J.K., Ermund, A., Birchenough, G.M.H., Schütte, A., van der Post, S., Svensson, F., Rodríguez-Piñeiro, A.M., Nyström, E.E.L., Wising, C., Johansson, M.E.V. and Hansson, G.C. (2014) 'The mucus and mucins of the goblet cells and enterocytes provide the first defense line of the gastrointestinal tract and interact with the immune system', *Immunological Reviews*, 260(1), pp. 8–20. Available at: https://doi.org/10.1111/imr.12182.

Peterson, G.L. (1979) 'Review of the folin phenol protein quantitation method of lowry, rosebrough, farr and randall', *Analytical Biochemistry*, 100(2), pp. 201–220. Available at: https://doi.org/10.1016/0003-2697(79)90222-7.

Peuhkuri, K., Vapaatalo, H. and Korpela, R. (2010) 'Even low-grade inflammation impacts on small intestinal function', *World Journal of Gastroenterology : WJG*, 16(9), pp. 1057–1062. Available at: https://doi.org/10.3748/wjg.v16.i9.1057.

Pietrzak, B., Tomela, K., Olejnik-Schmidt, A., Mackiewicz, A. and Schmidt, M. (2020) 'Secretory IgA in Intestinal Mucosal Secretions as an Adaptive Barrier against Microbial Cells', *International Journal of Molecular Sciences*, 21(23), p. 9254. Available at: https://doi.org/10.3390/ijms21239254.

Poelstra, K. and Bakker, W.W. (1997) 'Dephosphorylation of Endotoxin by Alkaline Phosphatase in Vivo', 151(4), p. 7.

Pound, L.D., Kievit, P. and Grove, K.L. (2014) 'The nonhuman primate as a model for type 2 diabetes', *Current Opinion in Endocrinology, Diabetes, and Obesity*, 21(2), pp. 89–94. Available at: https://doi.org/10.1097/MED.0000000000000043.

Pugin, J., Schürer-Maly, C.C., Leturcq, D., Moriarty, A., Ulevitch, R.J. and Tobias, P.S. (1993) 'Lipopolysaccharide activation of human endothelial and epithelial cells is mediated by lipopolysaccharide-binding protein and soluble CD14', *Proceedings of the National Academy of Sciences of the United States of America*, 90(7), pp. 2744–2748. Available at: https://doi.org/10.1073/pnas.90.7.2744.

Qin, X., Caputo, F.J., Xu, D.-Z. and Deitch, E.A. (2008) 'Hydrophobicity of mucosal surface and its relationship to gut barrier function', *Shock (Augusta, Ga.)*, 29(3), pp. 372–376. Available at: https://doi.org/10.1097/shk.0b013e3181453f4e.

Ragland, S.A. and Criss, A.K. (2017) 'From bacterial killing to immune modulation: Recent insights into the functions of lysozyme', *PLOS Pathogens*. Edited by J.B. Bliska, 13(9), p. e1006512. Available at: https://doi.org/10.1371/journal.ppat.1006512.

Regoli, M., Bertelli, E., Borghesi, C. and Nicoletti, C. (1995) 'Three-dimensional (3D-) reconstruction of M cells in rabbit peyer's patches: Definition of the intraepithelial compartment of the follicle-associated epithelium', *The Anatomical Record*, 243(1), pp. 19–26. Available at: https://doi.org/10.1002/ar.1092430104.

Rhee, S.H. (2014) 'Lipopolysaccharide: basic biochemistry, intracellular signaling, and physiological impacts in the gut', *Intestinal Research*, 12(2), pp. 90–95. Available at: https://doi.org/10.5217/ir.2014.12.2.90.

Riedel, S., Pheiffer, C., Johnson, R., Louw, J. and Muller, C.J.F. (2022) 'Intestinal Barrier Function and Immune Homeostasis Are Missing Links in Obesity and Type 2 Diabetes Development', *Frontiers in Endocrinology*, 12, p. 833544. Available at: https://doi.org/10.3389/fendo.2021.833544.

Roberts, S.J. and Hayday, A.C. (1996) 'T-cell aj3+ and yS3 deficient mice display abnormal but distinct phenotypes toward a natural, widespread infection of the intestinal epithelium', *Proc. Natl. Acad. Sci. USA*, (129), p. 6.

Roden, M. and Shulman, G.I. (2019) 'The integrative biology of type 2 diabetes', *Nature*, 576(7785), pp. 51–60. Available at: https://doi.org/10.1038/s41586-019-1797-8.

Rohr, M.W., Narasimhulu, C.A., Rudeski-Rohr, T.A. and Parthasarathy, S. (2019) 'Negative Effects of a High-Fat Diet on Intestinal Permeability: A Review', *Advances in Nutrition*, p. nmz061. Available at: https://doi.org/10.1093/advances/nmz061.

Rosenthal, R., Milatz, S., Krug, S.M., Oelrich, B., Schulzke, J.-D., Amasheh, S., Günzel, D. and Fromm, M. (2010) 'Claudin-2, a component of the tight junction, forms a paracellular water channel', *Journal of Cell Science*, 123(11), pp. 1913–1921. Available at: https://doi.org/10.1242/jcs.060665.

Saito, A.C., Higashi, T., Fukazawa, Y., Otani, T., Tauchi, M., Higashi, A.Y., Furuse, M. and Chiba, H. (2021) 'Occludin and tricellulin facilitate formation of anastomosing tight-junction strand network to improve barrier function', *Molecular Biology of the Cell*, 32(8), pp. 722–738. Available at: https://doi.org/10.1091/mbc.E20-07-0464.

Sakamoto, Y., Niwa, M., Muramatsu, K. and Shimo, S. (2021) 'High-Fat Diet and Age-Dependent Effects of IgA-Bearing Cell Populations in the Small Intestinal Lamina Propria in Mice', *International Journal of Molecular Sciences*, 22(3), p. 1165. Available at: https://doi.org/10.3390/ijms22031165.

Salvo Romero, E., Alonso Cotoner, C., Pardo Camacho, C., Casado Bedmar, M. and Vicario, M. (2015) 'The intestinal barrier function and its involvement in digestive disease', *Revista Española de Enfermedades Digestivas*, 108. Available at: https://doi.org/10.17235/reed.2015.3846/2015.

Sarker, S.A. and Gyr, K. (1992) 'Non-immunological defence mechanisms of the gut', *Gut*, 33(7), pp. 987–993. Available at: https://doi.org/10.1136/gut.33.7.987.

Sathaliyawala, T., Kubota, M., Yudanin, N., Turner, D., Camp, P., Thome, J.J.C., Bickham, K.L., Lerner, H., Goldstein, M., Sykes, M., Kato, T. and Farber, D.L. (2013) 'Distribution and Compartmentalization of Human Circulating and Tissue-Resident Memory T Cell Subsets', *Immunity*, 38(1), pp. 187–197. Available at: https://doi.org/10.1016/j.immuni.2012.09.020.

Schindelin, J., Arganda-Carreras, I., Frise, E., Kaynig, V., Longair, M., Pietzsch, T., Preibisch, S., Rueden, C., Saalfeld, S., Schmid, B., Tinevez, J.-Y., White, D.J., Hartenstein, V., Eliceiri, K., Tomancak, P. and Cardona, A. (2012) 'Fiji: an open-source platform for biological-image analysis', *Nature Methods*, 9(7), pp. 676–682. Available at: https://doi.org/10.1038/nmeth.2019.

Shah, P., Bao, Z. and Zaidel-Bar, R. (2022) 'Visualizing and quantifying molecular and cellular processes in Caenorhabditis elegans using light microscopy', *Genetics*, 221(4), p. iyac068. Available at: https://doi.org/10.1093/genetics/iyac068.

Shen, W., Wolf, P.G., Carbonero, F., Zhong, W., Reid, T., Gaskins, H.R. and McIntosh, M.K. (2014) 'Intestinal and Systemic Inflammatory Responses Are Positively Associated with Sulfidogenic Bacteria Abundance in High-Fat–Fed Male C57BL/6J Mice', *The Journal of Nutrition*, 144(8), pp. 1181–1187. Available at: https://doi.org/10.3945/jn.114.194332.

Sherwood, L. (2010) *Human physiology: from cells to systems / Lauralee Sherwood.* 7th ed. Australia ; United States: Brooks/Cole, Cengage Learning.

Shimazu, R., Akashi, S., Ogata, H., Nagai, Y., Fukudome, K., Miyake, K. and Kimoto, M. (1999) 'MD-2, a molecule that confers lipopolysaccharide responsiveness on Toll-like receptor 4', *The Journal of Experimental Medicine*, 189(11), pp. 1777–1782. Available at: https://doi.org/10.1084/jem.189.11.1777.

Shively, C.A., Appt, S.E., Vitolins, M.Z., Uberseder, B., Michalson, K.T., Silverstein-Metzler, M.G. and Register, T.C. (2019) 'Mediterranean versus Western Diet Effects on Caloric Intake, Obesity, Metabolism, and Hepatosteatosis in Nonhuman Primates',

Obesity (Silver Spring, Md.), 27(5), pp. 777–784. Available at: https://doi.org/10.1002/oby.22436.

de Sousa-Pereira, P. and Woof, J.M. (2019) 'IgA: Structure, Function, and Developability', *Antibodies*, 8(4), p. 57. Available at: https://doi.org/10.3390/antib8040057.

Spencer, J., Finn, T. and Isaacson, P.G. (1986) 'A comparative study of the gut-associated lymphoid tissue of primates and rodents', *Virchows Archiv. B, Cell Pathology Including Molecular Pathology*, 51(6), pp. 509–519. Available at: https://doi.org/10.1007/BF02899056.

Stanisic, D., Jeremic, N., Majumder, S., Pushpakumar, S., George, A., Singh, M. and Tyagi, S.C. (2021) 'High Fat Diet Dysbiotic Mechanism of Decreased Gingival Blood Flow', *Frontiers in Physiology*, 12, p. 625780. Available at: https://doi.org/10.3389/fphys.2021.625780.

Su, Y., Hong, Y., Mei, F., Wang, C., Li, M., Zhou, Y., Zhao, K., Yu, J. and Wang, W. (2019) 'High-Fat Diet Aggravates the Intestinal Barrier Injury via TLR4-RIP3 Pathway in a Rat Model of Severe Acute Pancreatitis', *Mediators of Inflammation*, 2019, pp. 1–13. Available at: https://doi.org/10.1155/2019/2512687.

Sun, W.W., Krystofiak, E.S., Leo-Macias, A., Cui, R., Sesso, A., Weigert, R., Ebrahim, S. and Kachar, B. (2020) 'Nanoarchitecture and dynamics of the mouse enteric glycocalyx examined by freeze-etching electron tomography and intravital microscopy', *Communications Biology*, 3(1), p. 5. Available at: https://doi.org/10.1038/s42003-019-0735-5.

Suzuki, T. and Hara, H. (2010) 'Dietary fat and bile juice, but not obesity, are responsible for the increase in small intestinal permeability induced through the suppression of tight junction protein expression in LETO and OLETF rats', *Nutrition & Metabolism*, 7(1), p. 19. Available at: https://doi.org/10.1186/1743-7075-7-19.

Tabara, Y., Arai, H., Hirao, Y., Takahashi, Y., Setoh, K., Kawaguchi, T., Kosugi, S., Ito, Y., Nakayama, T., Matsuda, F., and Nagahama study group (2017) 'Different inverse association of large high-density lipoprotein subclasses with exacerbation of insulin resistance and incidence of type 2 diabetes: The Nagahama study', *Diabetes*

Research and Clinical Practice, 127, pp. 123–131. Available at: https://doi.org/10.1016/j.diabres.2017.03.018.

Turner, J.R. (2009) 'Intestinal mucosal barrier function in health and disease', *Nature Reviews. Immunology*, 9(11), pp. 799–809. Available at: https://doi.org/10.1038/nri2653.

Van Itallie, C.M. and Anderson, J.M. (1997) 'Occludin confers adhesiveness when expressed in fibroblasts', *Journal of Cell Science*, 110 (Pt 9), pp. 1113–1121. Available at: https://doi.org/10.1242/jcs.110.9.1113.

Veenbergen, S. and Samsom, J.N. (2012) 'Maintenance of small intestinal and colonic tolerance by IL-10-producing regulatory T cell subsets', *Current Opinion in Immunology*, 24(3), pp. 269–276. Available at: https://doi.org/10.1016/j.coi.2012.03.004.

Velaga, S., Herbrand, H., Friedrichsen, M., Jiong, T., Dorsch, M., Hoffmann, M.W., Förster, R. and Pabst, O. (2009) 'Chemokine receptor CXCR5 supports solitary intestinal lymphoid tissue formation, B cell homing, and induction of intestinal IgA responses', *Journal of Immunology (Baltimore, Md.: 1950)*, 182(5), pp. 2610–2619. Available at: https://doi.org/10.4049/jimmunol.0801141.

Viriyakosol, S., Tobias, P.S., Kitchens, R.L. and Kirkland, T.N. (2001) 'MD-2 binds to bacterial lipopolysaccharide', *The Journal of Biological Chemistry*, 276(41), pp. 38044–38051. Available at: https://doi.org/10.1074/jbc.M105228200.

Wachtman, L.M., Kramer, J.A., Miller, A.D., Hachey, A.M., Curran, E.H. and Mansfield, K.G. (2011) 'Differential contribution of dietary fat and monosaccharide to metabolic syndrome in the common marmoset (Callithrix jacchus)', *Obesity (Silver Spring, Md.)*, 19(6), pp. 1145–1156. Available at: https://doi.org/10.1038/oby.2010.303.

Wershil, B. and Furuta, G. (2008) '4. Gastrointestinal mucosal immunity', *Journal of Allergy and Clinical Immunology*, 121(2), pp. S380–S383. Available at: https://doi.org/10.1016/j.jaci.2007.10.023.

Willett, M. (2019) 'An introduction to image processing using ImageJ'. Imaging and Microscopy Centre, Centre for Biological Sciences, University of Southampton.

Available   at:
https://www.southampton.ac.uk/~assets/doc/Processing%20workshop.pdf.

Williams, I.R. (2006) 'CCR6 and CCL20: partners in intestinal immunity and lymphorganogenesis', *Annals of the New York Academy of Sciences*, 1072, pp. 52–61. Available at: https://doi.org/10.1196/annals.1326.036.

Wilson, K. and Walker, J.M. (2010) *Principles and techniques of biochemistry and molecular biology*. 7th ed. Cambridge (Mass.): Cambridge university press.

Winer, D.A., Winer, S., Dranse, H.J. and Lam, T.K.T. (2017) 'Immunologic impact of the intestine in metabolic disease', *The Journal of Clinical Investigation*, 127(1), pp. 33–42. Available at: https://doi.org/10.1172/JCI88879.

Woof, J.M. and Russell, M.W. (2011) 'Structure and function relationships in IgA', *Mucosal Immunology*, 4(6), pp. 590–597. Available at: https://doi.org/10.1038/mi.2011.39.

Worthington, J.J. (2015) 'The intestinal immunoendocrine axis: novel cross-talk between enteroendocrine cells and the immune system during infection and inflammatory disease', *Biochemical Society Transactions*, 43(4), pp. 727–733. Available at: https://doi.org/10.1042/BST20150090.

Xepapadaki, E., Nikdima, I., Sagiadinou, E.C., Zvintzou, E. and Kypreos, K.E. (2021) 'HDL and type 2 diabetes: the chicken or the egg?', *Diabetologia*, 64(9), pp. 1917–1926. Available at: https://doi.org/10.1007/s00125-021-05509-0.

Xie, Y., Ding, F., Di, W., Lv, Y., Xia, F., Sheng, Y., Yu, J. and Ding, G. (2020) 'Impact of a high‑fat diet on intestinal stem cells and epithelial barrier function in middle‑aged female mice', *Molecular Medicine Reports*, 21(3), pp. 1133–1144. Available at: https://doi.org/10.3892/mmr.2020.10932.

Yu, T., Wang, Y., Chen, X., Xiong, W., Tang, Y. and Lin, L. (2020) 'Spirulina platensis alleviates chronic inflammation with modulation of gut microbiota and intestinal permeability in rats fed a high-fat diet', *Journal of Cellular and Molecular Medicine*, 24(15), pp. 8603–8613. Available at: https://doi.org/10.1111/jcmm.15489.

Zeuthen, L.H., Fink, L.N. and Frokiaer, H. (2008) 'Epithelial cells prime the immune response to an array of gut-derived commensals towards a tolerogenic phenotype through distinct actions of thymic stromal lymphopoietin and transforming growth factor-beta', *Immunology*, 123(2), pp. 197–208. Available at: https://doi.org/10.1111/j.1365-2567.2007.02687.x.

Zheng, Y. and Rudensky, A.Y. (2007) 'Foxp3 in control of the regulatory T cell lineage', *Nature Immunology*, 8(5), pp. 457–462. Available at: https://doi.org/10.1038/ni1455.

Zhou, B., Lu, Y., Hajifathalian, K., Bentham, J., Di Cesare, M., Danaei, G., Bixby, H., Cowan, M.J., Ali, M.K. and Taddei, C. (2016) 'Worldwide trends in diabetes since 1980: a pooled analysis of 751 population-based studies with 4· 4 million participants', *The Lancet*, 387(10027), pp. 1513–1530.

APPENDICES

6. List of appendices

6.1. Appendix A: Equipment and software

Table 6.1: List of equipment and software used in the study

Equipment and software	Company name and country of origin
Leica TP1020 Automatic Tissue Processor	Leica Biosystems, USA
Leica RM2125 RT Rotary Microtome	
Stuart™ Microtitre Plate Shaker Incubator	Cole-Parmer, USA
TISSUE-TEK® embedding station	Sakura Finetek, USA
Nikon Eclipse Ti-S	Nikon, Japan
Nikon Ti-PS100W/A light source	
Nikon DS-Fi1c camera	
Nikon Digital Sight DS-U3	
Prior ProScan III	Prior Scientific Instruments Ltd, UK
DakoCytomation Pascal Pressure Chamber	Agilent Technologies Inc, USA
LSM78 with ELYRA PS1 confocal microscope	Carl Zeiss, Germany
Andor EM-CCD camera iXon DU 897 for PALM/STORM	
Qiagen MM300 Mixer Tissue Lyser	Qiagen, USA
Trans-Blot Cell	Bio-Rad Laboratories, South Africa
Mini-PROTEAN® Tetra Cell, Mini Trans-Blot® Module, and PowerPac™ HC Power Supply (#1658035)	
ChemiDoc MP Imaging System	
Image Lab (version 6.1.0 build 7)	
Prism™ R Refrigerated Microcentrifuge	Labnet International, USA
Spectramax i3 Multimode Plate Reader	Molecular Devices, USA
IKA MS 3 Digital	IKA-Werke GmbH & Co. KG, Germany
NIS-Elements software version 4.51.00 Build 1143	Laboratory Imaging s.r.o., Czech Republic
Fiji Is Just ImageJ (FIJI) 1.53t	National Institutes of Health, USA
GraphPad Prism 8 for Windows Version 8.4.2	Graphpad Software, USA
Microsoft 365 Apps for enterprise	Microsoft Corporation, USA

6.2. Appendix B: Reagents and consumables

Table 6.2: List of reagents and consumables used in the study

Reagents and consumables	Manufacturer and country
Immobilon-P PVDF Membrane #PVH15150	Merck, Germany
Hydrochloric acid (HCL) solution (#30721)	
Sodium Hydroxide (NaOH) (#30620)	
Citric acid ($C_6H_8O_7.H_2O$) (#3013284)	
Sodium citrate ($C_6H_5Na_3O_7.2H_2O$) (#1.166448.0500)	
Tris (hydroxymethyl aminomethane) (#1.08382.0500)	
Sodium chloride (NaCl) (#1.06404.0500)	
Sodium dihydrogen orthophosphate (NaH_2PO_4) (#AB006580.500g)	
Disodium hydrogen orthophosphate (Na_2HPO_4) (#1.06559.0500)	
Sodium azide (#6688)	
Methanol (#34860)	
Haematoxylin (#H9627)	
Eosin Y-solution 0.5% aqueous (#109844)	
Ammonium aluminium sulphate dodecahydrate (#A2140-5009)	
Entellan rapid mounting medium (#1.07960)	
Phosphatase inhibitors (#4906845001)	
Protease inhibitors (#5892953001)	
β- Mercaptoethanol # M3148	
TEMED (#T7024)	
Ammonium persulfate (APS) (#09914)	
Bisbenzimide Hoechst 33342 (#B2261)	
Ponceau S stain (#P7170)	
Tween-20 (#P2287)	
Glycine (#G7126)	
Acetic acid solution (#27225)	
Triton X-100 (#30632)	
Sodium dihydrogen orthophosphate dihydrate ($NaH_2PO_4.2H_2O$), (#301324Q)	VWR Chemicals BDH, USA
HistoBond adhesive microscope slides #0810000	

Glass coverslips	Paul Marienfeld GmbH & Co.KG, USA
Fluorescent mounting media (Dako) #S3023	Agilent Technologies USA
10% Neutral buffered formalin	Laborem Lab Supplies, South Africa
Xylene #6238	UN Lab, South Africa
p44/42 MAPK (ERK1/2) (137F5) rabbit mAb #4695	Cell Signaling Technology, South Africa
Phospho-p44/42 MAPK (ERK1/2) (Thr202/Tyr204) antibody #9101	
Anti-rabbit IgG, HRP-linked antibody #7074	
Mouse IgA antibody # NBP2-61794	
Occludin monoclonal antibody (OC-3F10) (#33-1500)	Thermo Fisher Scientific, USA
Cell lysis buffer (#FNN0011)	
Rhesus Monkey CD14 ELISA kit (#EP21RB)	
Alexa Fluor 488 AffiniPure donkey anti-mouse IgG (H+L) (#715-545-150)	Jackson ImmunoResearch, USA
TGX Stain-Free FastCast™ acrylamide kit, 12% #1610185	Bio-Rad, USA
DC Protein assay kit II (#5000112)	
Clarity western ECL substrate, 500 mL #1705061	
Precision Plus Protein WesternC blotting standards, 250 µl #1610376	
Precision Protein StrepTactin-HRP conjugate, 300 µl #1610380	
10x Tris/ Glycine/ SDS electrophoresis buffer #1610772	
2X Laemli sample buffer #1610737	
Coomassie Brilliant Blue R250 #1610400	
Monkey Lipopolysaccharide Binding Protein (LBP) ELISA Kit (#E-EL-MK0696)	Elabscience, USA

6.3. Appendix C: Buffers and solutions

Table 6.3: List of buffers and solutions used in the study

Buffers and solutions	Preparation
Haematoxylin (1L)	• Added 50 g of ammonium aluminium sulphate with 1L of distilled water (mixed until dissolved) • Added 1 g haematoxylin to the solution (mixed until dissolved) • Added 0.2 g of $NaIO_3$ (mixed until dissolved) • Added 1 g of citric acid (mixed until dissolved)
0.05 M Tris buffered saline (TBS) pH 7.2 (5L)	• 30.284 g of Tris and 42.5 g of NaCl in 4700 mL dH_2O • Adjusted pH to 7.2 with HCl • Adjusted final volume to 5000 mL with dH_2O
0.05 M Tris buffered saline (TBS) pH 7.2 with 0.5% Triton X-100 (1L)	• Added 5 mL of Triton X-100 to 995 mL of 0.05 M TBS pH 7.2
0.1 M Phosphate buffered saline (PBS) pH 7.2	• Added 3.12 g of NaH_2PO_4 in 100 mL dH_2O (stock A) • Added 14.15 g of Na_2HPO_4 in 1000 mL dH_2O (stock B) • Added 9.5 mL of stock A and 40.5 mL of stock B and made up to 90 mL dH_2O • Added 0.85 g NaCl and adjusted pH to 7.2 • Made up to 100 mL with dH_2O. • Added 0.1 g of BSA and 0.01 g of NaN_3 • Mixed with a magnetic stirrer until dissolved
Normal donkey serum	• Whole donkey blood in SST tubes was centrifuged for 15 minutes at 152 x g • Serum was separated into microcentrifuge tubes which were placed in a waterbath (60°C) for 30 minutes • 65 µl of the serum was added to 1235 µl of 0.1 M PBS pH 7.2 on the day of use
0.01 M Citrate buffer pH 6.0 (1L)	• 2.01 g of citric acid ($C_6H_8O_7$) was added in 100 mL dH_2O (stock A) • 29.41 g tri-sodium citrate ($Na_3C_6H_5O_7$) was added in 1L dH_2O (stock B) • Added 5 mL of stock A and 95 mL of stock B • Adjusted pH to 6.0 with HCl/ NaOH • Adjusted final volume to 1000 mL with dH_2O
Cell lysis buffer (100 mL) (#FNN0011)	• Buffer formulation: 10 mM Tris, pH 7.4, 100 mM NaCl, 1 mM EDTA, 1 mM EGTA, 1 mM NaF, 20 mM $Na_4P_2O_7$ 2 mM Na_3VO_4, 1% Triton X-100, 10% glycerol, 0.1% SDS, 0.5% deoxycholate • Added 10 phosphatase inhibitor cocktail tablets (#4906845001, Merck, Germany) to cell lysis buffer

	• Added 2 protease inhibitor cocktail tablets (#5892953001, Merck, Germany) to cell lysis buffer
Transfer buffer (1L)	• Added 3.03 g of Tris and 14.41 g Glycine in 800 mL of dH_2O • Added 200 mL (20%) of methanol
10X TBS (pH=7.6) (1L)	• Added 24.22 g of Tris and 80.06 g of NaCl in 800 mL of dH_2O & dissolved by mixing with a magnetic stirrer • Adjusted pH to 7.6 with HCl/ NaOH • Adjusted final volume to 1L with dH_2O
1X TBST	• Diluted 100 mL of 10X TBS in 900 mL dH_2O and added 1 mL Tween-20

6.4. Appendix D: Demographic data of vervet monkeys

Table 6.4: Demographic data of vervet monkeys (*Chlorocebus aethiops*)

Diet group	Monkey ID	Date of birth	Age	Gender	Euthanisation date
Maize-based diet	M1068	Wild-caught	23	Male	18 October 2017
	M136	01 February 1995	21	Female	25 October 2017
	M1077	Wild-caught	21	Male	09 January 2018
High-fat diet	M39	19 October 1989	27	Female	18 August 2017
	M49	27 August 1990	26	Female	02 August 2017
	M92	07 November 1993	23	Female	29 August 2017
	M141	26 October 1995	21	Female	04 January 2018
	M1082	Wild-caught	21	Male	18 January 2018
	M1083	Wild-caught	21	Male	11 May 2017

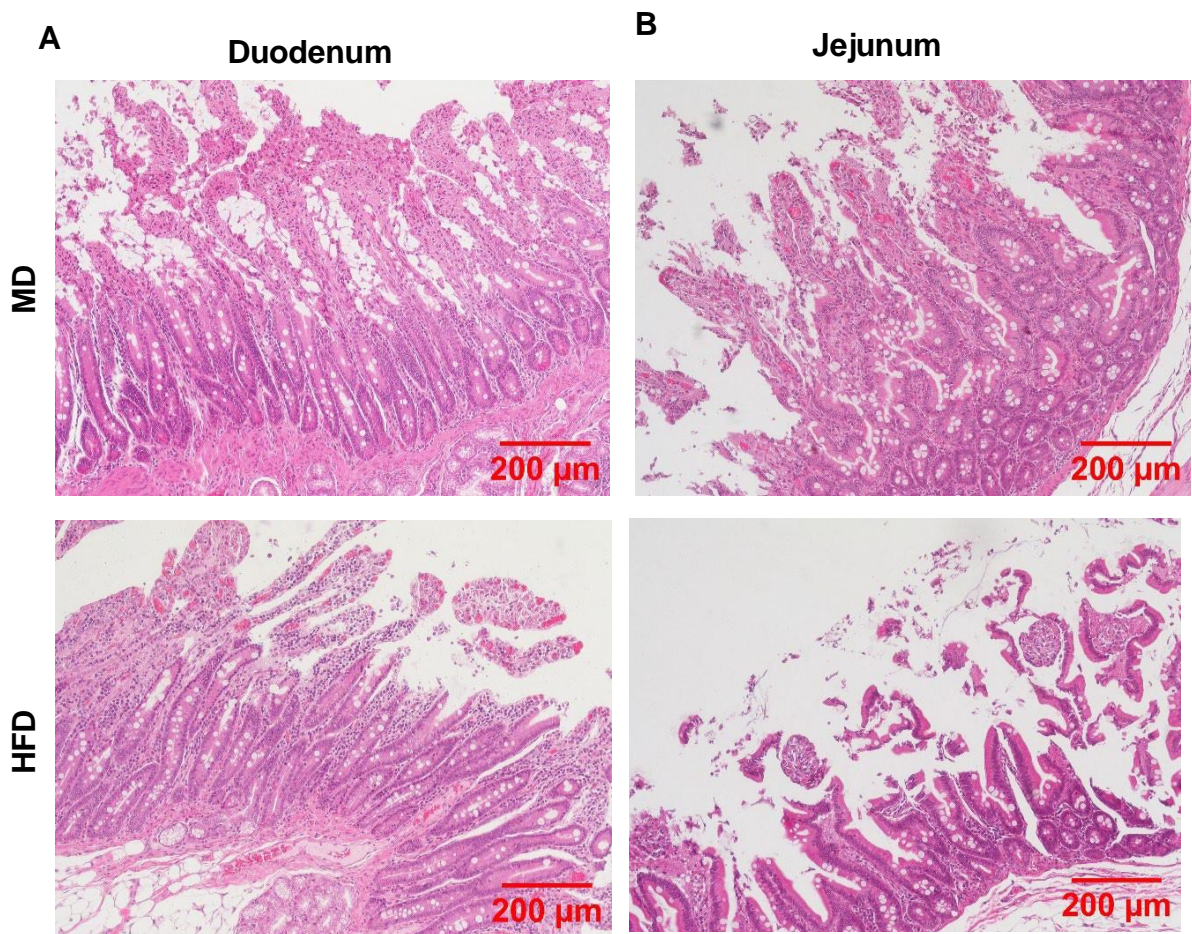## 6.5. Appendix E: Autolysed duodenum and ileum sections

Figure 6.1: Autolysis of intestinal tissues of vervet monkeys *(Chlorocebus aethiops).* Representative images depicting autolysed duodenum **(A)** and jejunum **(B)** tissues of MD-fed and HFD-fed vervet monkeys. Abbreviations: maize-based diet (MD) and high-fat diet (HFD).

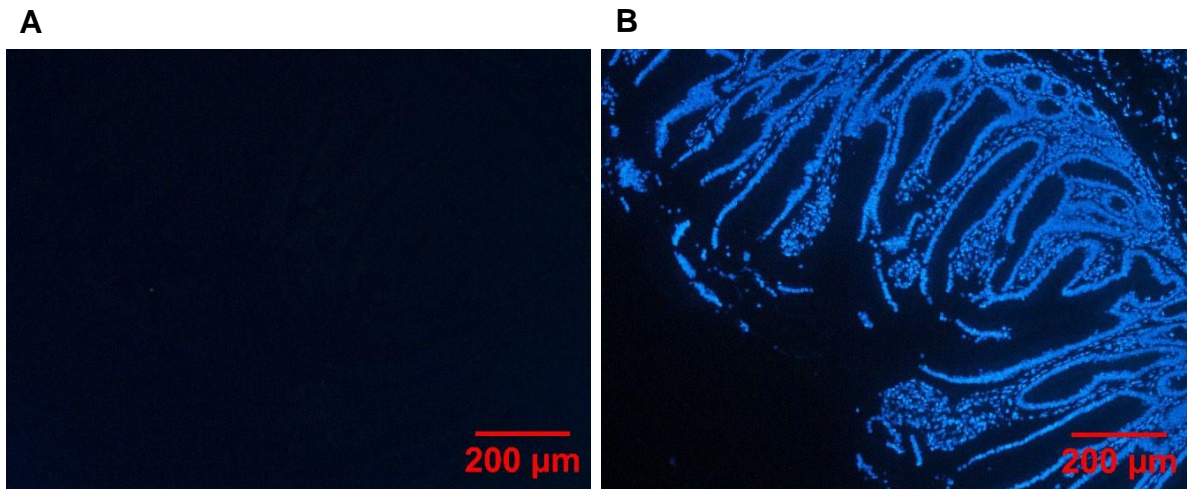## 6.6. Appendix F: Negative control images for immunohistochemistry

A

B

Figure 6.2: Negative control for IgA$^+$ cells in intestinal tissue area of vervet monkeys (*Chlorocebus aethiops*). Representative multi-channel images depicting the absence of IgA$^+$ cells **(A)** in intestinal tissue **(B)** of vervet monkeys.

6.7. Appendix G: Total protein images from western blot analysis

A

D
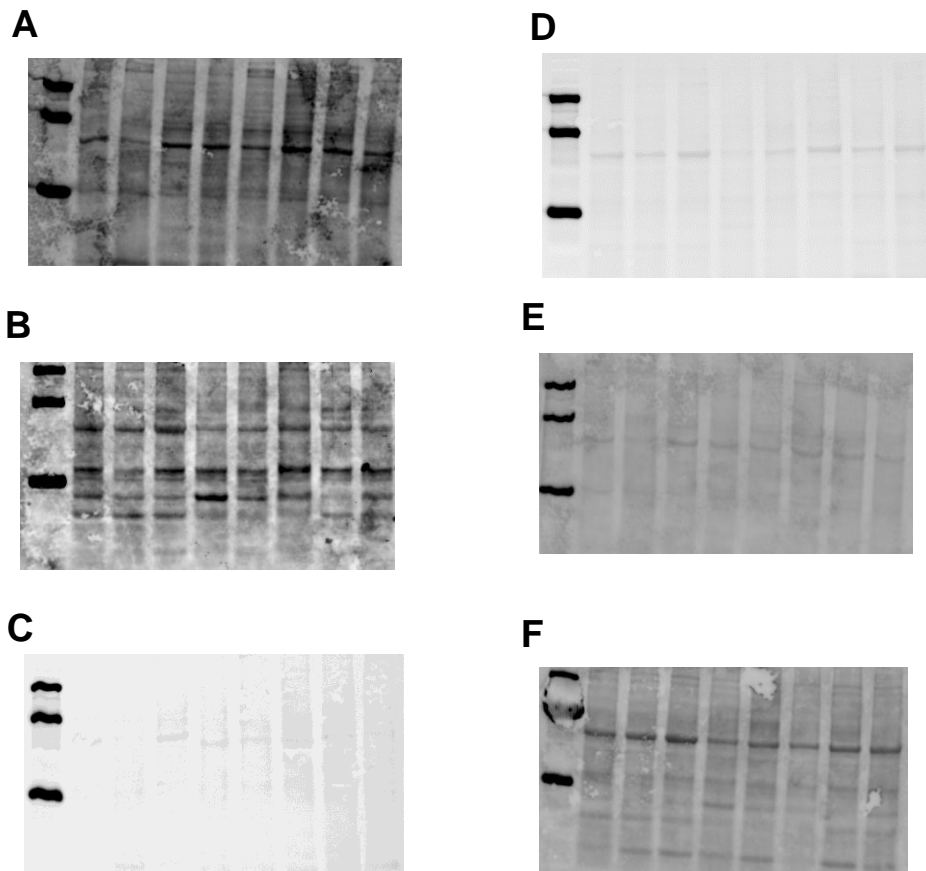

B

E

C

F

Figure 6.3: Total protein images of polyvinylidene fluoride membranes. Imaged were acquired using ChemiDoc MP Imaging System for normalisation of phosphorylated-ERK in the ileum **(A)** and colon **(B)**, total-p38 in the ileum **(C)** and colon **(D)**, total-ERK in the ileum **(E)** and colon **(F)** using Image Lab software.

6.8. Appendix H: List of antibodies that did not work in for the western blot experiments

Table 6.5: List of primary antibodies that could not be detected in intestinal tissues of vervet monkeys (*Chlorocebus aethiops*) using western blots

Antibody name and catalog number	Dilution(s) used	Supplier and country
Phospho-NF-κB p65 (Ser536) (93H1) rabbit mAb #3033	1:1000 and 1:500	Cell Signaling Technology, South Africa
NF-κB p65 (D14E12) XP® rabbit mAb #8242	1:1000 and 1:500	
ZO-1 (D6L1E) rabbit mAb #13663	1:1000	
ZO-1 (D7D12) rabbit mAb #8193	1:1000	
Phospho-Akt (Ser473) (D9E) XP® rabbit mAb #4060	1:1000	
Akt (pan) (C67E7) rabbit mAb #4691	1:1000	
SAPK/JNK antibody #9252	1:1000	
Recombinant anti-MyD88 antibody [EPR21824] #ab219413	1:1000	Abcam, UK
Anti-COX2 / cyclooxygenase 2 antibody (ab52237)	1:1000	
Mouse IgA antibody #NBP2-61794	1:1000	Novus Biologicals, USA